3-2023

Modeling Radiation Exposure on Flight Missions to Analyze Aircrew Risk

Camila V. Quintero Hilsaca

MODELING RADIATION EXPOSURE ON FLIGHT MISSIONS TO ANALYZE AIRCREW RISK

THESIS

Camila V. Quintero Hilsaca, Second Lieutenant, USAF

AFIT-ENP-MS-23-M-101

DEPARTMENT OF THE AIR FORCE
AIR UNIVERSITY

AIR FORCE INSTITUTE OF TECHNOLOGY

Wright-Patterson Air Force Base, Ohio

AFIT-ENP-MS-23-M-101

MODELING RADIATION EXPOSURE ON FLIGHT MISSIONS TO ANALYZE AIRCREW RISK

THESIS

Presented to the Faculty

Department of Engineering Physics

Graduate School of Engineering and Management

Air Force Institute of Technology

Air University

Air Education and Training Command

in Partial Fulfillment of the Requirements for the

Degree of Master of Science in Nuclear Engineering

Camila V. Quintero Hilsaca, B.S.

Second Lieutenant, USAF

March 23, 2023

AFIT-ENP-MS-23-M-101

MODELING RADIATION EXPOSURE ON FLIGHT MISSIONS TO ANALYZE AIRCREW RISK

THESIS

Camila V. Quintero Hilsaca, B.S.
Second Lieutenant, USAF

Committee Membership:

Dr. John McClory,
Chair

Dr. Juan J. Manfredi,
Member

Lt Col Whitman Dailey, Ph.D
Member

Abstract

Galactic cosmic rays and solar particle events comprise the majority of the ionizing radiation experienced in the upper atmosphere within flight-altitude environments. Although previous studies have analyzed radiation doses from single sources on civilian flight operations, there is a lack of research focused on dose received by military personnel during flight from both sources simultaneously. In-flight radiation environments are modeled through the Monte Carlo N-Particle (MCNP6) code for two separate aircraft: an Air Force A-10 and a Boeing 737. Particle fluence values for galactic cosmic rays and solar particle events for four separate flight paths are determined using the CARI-7A software and the SIRE2 toolkit, respectively. MCNP6 code and flux-to-dose conversion factors from the International Commission on Radiological Protection Publication 60 were used to determine the effective dose received by aircrew. The effective dose for each flight was compared to the effective dose provided by the CARI-7A software and the SIRE2 toolkit. Overall, the results for galactic cosmic rays and solar particle events doses through the simulated environment matched the CARI-7A software results better than the SIRE2 toolkit results. The SIRE2 toolkit predicted no particle fluence for the two flight tracks through the equator and an effective dose of 23,760 μSv for a flight path near the Arctic circle during a solar maximum. Additionally, for the Boeing 737 the effective dose for a passenger in the middle of the plane was approximately half of the effective dose for the pilot at the front of the aircraft. Finally, a A-10 pilot received approximately 10 times the dose of a Boeing 737 pilot.

Acknowledgements

I want to thank my faculty advisor, Dr. John McClory, for his support through this entire process. The freedom he granted me to pursue and explore different avenues for this research project made my time at AFIT extremely rewarding. His guidance through the roadblocks as well as his flexibility and understanding were huge contributors to my success. I would also like to thank the rest of my committee, Lt Col Whitman Dailey and Dr. Juan Manfredi, for devoting their time and expertise to this project. Additionally, I would like to thank Dr. William Erwin at the Air Force School of Aerospace Medicine for conceiving the start of this project and for his continuous support through the program. Finally, to my partner for his patience and love through this program. Thank you for pushing and encouraging me every day.

Camila V. Quintero Hilsaca

Table of Contents

Page

List of Figures

Figure Page

List of Tables

MODELING RADIATION EXPOSURE ON FLIGHT MISSIONS TO ANALYZE AIRCREW RISK

I. Introduction

1.1 Overview

In 1994 the Federal Aviation Administration (FAA) formally recognized ionizing radiation became one of the major environmental factors of concern to the health and safety of military pilots [1]. Ionizing radiation is the interaction between subatomic particles, ionized atoms, or energetic photons and an atom that causes the atom itself to lose an electron or break apart, i.e. ionize [2]. These interactions within the human body can cause a wide range of health problems divided into deterministic and stochastic effects.

Deterministic health effects are defined as those which occur after a threshold is met; therefore, below this limit the person should not experience that particular effect. Skin erythema, irreversible skin damage, hair loss, sterility, fetal abnormality, and lethality are examples of deterministic effects. Specifically for a pregnant aviator or flight crew member, tracking this radiation limit (0.1 – 0.5 Gy [3]) during flights is critical for the overall health and well-being of the aviator. With stochastic effects, the probability of the effect occurring increases with dose while the severity remains stagnant. These effects can develop over both short and long periods of time, allowing the person to remain unaware of its impact until years later. In contrast to deterministic effects, stochastic effects do not have a minimum threshold to be considered unsafe [3]. Cancers and genetic defects are some examples of stochastic effects.

Although ionizing radiation can still be present at ground level, the magnitude of exposure rises significantly within flight-altitude environments as these altitude levels encounter a specific type of ionizing radiation stemming from outer space called cosmic ionizing radiation. This type of ionizing radiation includes galactic cosmic radiation (GCR) and solar particle events (SPE).

Galactic cosmic radiation originates outside of the solar system and most likely stems from explosive events such as supernovae. GCR generally consists of ions, protons, neutrons, electrons, positrons, photons, and muons. At flight altitudes most of the dose depends on the protons and neutrons [4]. All these particles are highly energetic and the ions, protons, positrons, electrons, and muons are charged making them susceptible to interactions with and influence from the existing magnetic fields [5]. Both the Sun's and the Earth's magnetic fields partly modulate the GCR's flux at the Earth's atmosphere. Ionized particles are deflected based on their direction's perpendicular component to the Earth's magnetic field, meaning particles are further deflected at the equator than they are at the poles [6]. This indicates that the intensity of GCR increases as a function of increasing latitude. Additionally, together the primary incident particles and the secondary radiation produced through interactions with the Earth's atmosphere generate increasing radiation exposure with altitude [6]. Not only is GCR perturbed by the atmosphere, but also the solar modulations and activity (to include solar flares and coronal mass ejections) affect the intensity of this type of ionizing radiation. Cosmic radiation is dependent on the solar cycle with periods of low solar activity, namely Forbush decreases, decreasing its intensity [6]. Forbush decreases represent the sudden decrease of GCRs by 3% to 20% lasting minutes to hours followed an increase to its previous intensity lasting hours or days [7]. This phenomenon is well understood and researched with many dedicated efforts at tracking its effects on humans.

Solar particle events occur when the Sun releases large amounts of energetic particles consisting mostly of protons along with alpha particles and heavier ions [8]. These particles are accelerated either right after their ejection from the Sun by a solar flare (SF) or subsequently by coronal mass ejection shocks (CMES). Therefore, SPE can be differentiated into two categories: impulsive events driven by SFs and gradual events driven by CMES [9]. Impulsive events produce a stream of high-energy particles which travel along the interplanetary magnetic field lines connected to the flare site. Gradual events cause these particles to interact with shock waves which propagate in all directions and travel along a broad number of interplanetary magnetic field lines, expanding the longitudinal effect. Because of their expansive range, it is believed that most of the SPE effects felt on Earth are caused by gradual events [9]. The frequency of SPE varies yet is dependent on the level of activity from the Sun relative to its 11-year cycle. Throughout an event, the intensity as well as the energy spectrum of emitted particles vary over time, making the trajectory and energy of these particles difficult to predict. The 1859 Carrington event marked the first and largest solar particle event ever recorded [10]. During this event, scientists witnessed extraordinary magnetic disturbances that affected almost half of the telegraphic stations in the United States. Additionally, citizens in Cuba, Jamaica and Panama even witnessed auroras in their regions, a phenomena typically only visible near the poles [11].

Although not originating from space, terrestrial gamma flash (TGF) is another form of ionizing radiation present within flight-altitudes. TGFs are bright bursts of multi-energy gamma-ray emissions produced as a result of thunderclouds and lightning. These high-energy photons interact with the air and produce low-energy electrons and ions, increasing the conductivity of the environment [12]. Because lightning can occur from the charge attraction between clouds to air, clouds to ground,

intracloud (within the clouds) and intercloud (clouds to clouds) [13], aircraft flying anywhere near a thunderstorm could experience this type of radiation. Although the discovery and understanding of this phenomenon is relatively new and limited, many TGFs have already been observed and measured in the past decade. The majority of these TGFs were associated with single lightning events; however, they have only been detected in a minority of the total lightning events measured [14] [15]. Some of the TGFs did not have any lighting discharge associated with their detection [15]. Currently, there are efforts to capture TGF data with specialized radiation detectors on WC-130 aircraft from the 53rd Reconnaissance Weather Squadron; however, the results of this work have not been published.

Currently, most of the advice given to pilots and aircrew for minimizing the risk of exposure to ionizing radiation is to work fewer hours or to fly shorter flights at lower altitudes. Because of the nature of the military's mission, these two solutions are either impractical to implement or only possible if there is significant data showing that aircrew's intake of radiation surpasses the recommended standard. Utilizing computational tools to determine projected effective dose for pilots and aircrew on a particular fight path at a particular flight time could inform mission planning in order to minimize health risks to personnel.

1.2 Motivation & Problem Statement

There is currently a lack of active understanding involving the integration of all types of ionizing radiation through an aircraft as well as its effects on military crew. While previous studies have touched on radiation dosages concentrating on one source [4] [6] [8] [16] [17] [18] [19], none have studied the effects of all sources simultaneously. Additionally, while much of the computational research surrounding this topic has been devoted to measuring dose through a flight path [20] [21], none had studied

the outcome of this radiation interacting through aircraft of various types on its crew members. The unknown manner by which these upper atmospheric particles transport their energy through an aircraft and the crew generates a unique risk to those military members. In 2019, the United States Air Force updated their policy on pregnant aviators extending their flying period to the end of the third trimester [22]. This permission is granted to any pilots who wish to continue flying pending approval from their obstetrician, flight surgeon, and commander. Despite this improvement in policy, there is still a lack of information given to pilots on their radiation intake to better inform their decision to continue or stop their flying duties while pregnant. This research aims to integrate all forms of cosmic ionizing radiation in flight-altitude environments into one model that outputs dose to military pilots and aircrew within a specific aircraft on a specific flight path. This will help characterize not only the flight-altitude environments but also study particle energy transport through the aircraft until it reaches aircrew. With this information we can assess and mitigate any potential health risks that military aircrew and pilots might endure during flight.

1.3 Brief Description of Computational Approach

My approach started with the selection of two flight trajectories, one through the higher temperate latitudinal zone and another through the middle of the tropic latitudinal zone. In addition to two distinct trajectories, I also had two different dates for each flight path, one during a solar minimum day and another through a solar maximum day of the same solar cycle. Afterwards, I imported the flight information into the Civil Aviation Research Institute (CARI-7A) software and the Space Ionizing Radiation Environment and Effects (SIRE2) toolkit to acquire the fluence values (in units of particles per square centimeter) from the GCR and SPE radiation, respectively, for each specific flight. Because these values vary with flight

path and date of flight, I ran the simulations through each different tool consistent with the original flight data. Afterwards, I created several Monte Carlo N-Particle Transport Code (MCNP) input decks using Software for Optimization of Radiation Detectors (SWORD) with two plane types, a Boeing 737 and an A-10, with flight crew inside. The personnel inside the planes functioned as detectors, taking a tally count of the particles that interact with them. Additionally, these input decks also contained a spherical isotropic source consistent with each type of radiation found from the simulations. I ran these input decks through MCNP to calculate the dose rate per source particle received by each chosen person in the aircraft from each source particle. Using the fluence values from CARI-7A and SIRE2, the length of each flight, and the dose rate values from MCNP, I evaluated the final total dose for each person, simulating the dose received by a flight crew during a military flight.

1.4 Assumptions & Limitations

For this project I only used publicly available data for both the aircraft design and flights paths, minimizing the overall data sensitivity of the research. While I acknowledge the significance of modeling realistic flight paths as well as aircraft on the eventual application, this proof of concept study does not require that level of specificity and detail. Therefore, I will make necessary assumptions about the aircraft designs as well as flight path information throughout the project to maintain my research and results at the theoretical level.

Additionally, uncertainties in the specified conditions that result in TGFs as well as the lack of data available have prevented the creation of a computational program such as CARI-7A and SIRE2 that could output the fluence values created by this type of radiation during a flight. Therefore, instead of creating an estimate of the fluence from TGFs with an extremely high factor of uncertainty, I have decided to

forgo this contribution to the dose calculation completely; however, I wrote my source input decks in a generic format so that future values of TGF fluence could be easily implemented into my code.

II. Background and Literature Review

2.1 Terminology

Radiation exposure defines the absorption of ionizing radiation either through ingestion, inhalation, or contact with the skin in units of Roentgen [23]. Dose specifies the amount of absorption measured distinctly through absorbed dose, equivalent dose, and effective dose. Absorbed dose represents the total amount of energy deposited into human tissue from ionization radiation exposure [24]. This value is used to assess the potential change that may occur to the exposed tissue. Absorbed dose is measured in units of Gray (Gy) or rad. Equivalent dose takes the previous definition a step forward by accounting for the type of radiation depositing energy into the tissue [24] Biological effects vary depending on the type of radiation the tissue is exposed to. Equivalent dose is measured in units of Sievert (Sv) or rem. Finally, effective dose takes into account the amount of energy, the type of radiation and the type of tissue [24] This value is used to assess the potential long-term risks from certain activities or procedures, such as background radon exposure or computed tomography (CT) scans. Effective dose is measured in the same units as equivalent dose.

On average an adult in the United States receives an annual dose of 0.62 rem [25]. Around 50 percent of this intake stems from natural background source including radon gas or radiation from space. Medical procedures, including X-ray scans, or nuclear medicine, including cancer treatments, make up 48 percent. Finally, 2 percent is attributed to occupational tasks, research exposure or product usage. The National Council on Radiation Protection and Measurements deems this level of exposure harmless to humans and sets the annual dose limit to 5 rem or 50 mSv [25].

2.2 Galactic Cosmic Radiation

Although the content and effects of galactic cosmic radiation are well understood, there is still no clear answer to the nature of its origin [26]. In the early 1930s, scientists theorized an the association between cosmic rays and supernova explosions when they determined that the energy density of cosmic rays could be supplied by just 10% of the energy from supernovae. It was not until the 1970s that scientists were able to quantitatively prove this energy conversion phenomena [27]. Now, there is enough evidence to definitively say galactic cosmic rays originate outside of the solar system from explosive events such as supernovae [5].

In the solar system, GCR consists mostly of protons (88%), alpha particles (11%), electrons (2%), and heavier nuclei ($\sim$1%) with energies ranging up to over 10^{14} MeV [6]. Once these particles reach the atmosphere, they interact with the nitrogen and oxygen species in this environment and produce lower Z nuclei, secondary protons, neutrons, and charged and uncharged pions. These secondary protons and neutrons generate even more protons and neutrons, known as a hadron cascade. At lower altitudes, around 10 km, the neutrons in the hadron cascade dominate because of their longer free mean path. The uncharged pions decay to high energy photons producing electron-positron pairs which annihilate to photons and further produce electron-positron pairs, known as an electron-photon cascade. Finally, the charged ions produce muons, known as a muon cascade, which further decay increasing the population of electrons and positrons [6]. All three types of cascades are displayed in Fig. 1. The particle composition, i.e. the percent value for each particle, changes depending on the altitude within the atmosphere. At temperate zone latitudes and typical aircraft altitudes the particle breakdown is as follows: 55% neutrons, 20% electrons and positrons, 15% protons, 5% photons, and 5% muons [6]. Additionally, at this altitude energetic primary heavy charged particles are not significant to the

dose calculations.

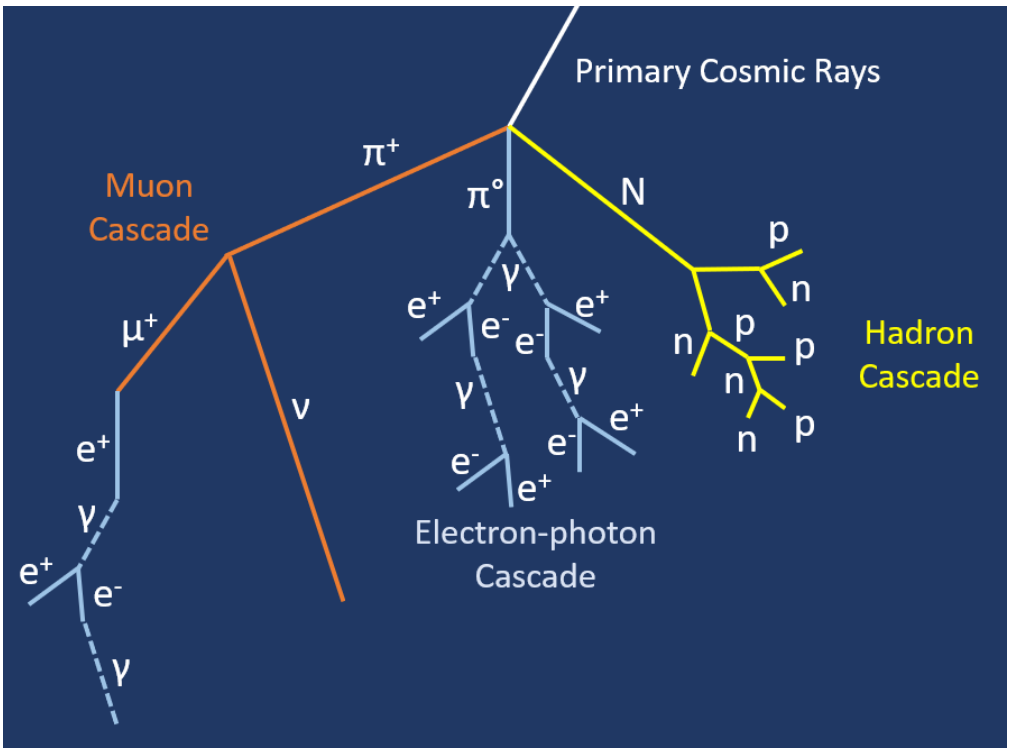

Figure 1: Development of particle cascades [electron-photon cascade (blue), muon cascade (orange), and hadron cascade (yellow)] from primary galactic cosmic radiation particles [28].

Aside from the location within the atmosphere, the effects of GCR also differ over the course of the 11-year solar cycle [5]. During a solar minimum, where there is an absence of coronal mass ejections and their corresponding magnetic fields, higher amounts of GCR particles can penetrate through the atmosphere. On the other hand, during a solar maximum the solar wind decreases the amount of lower-energy GCR that penetrates to Earth. Overall, GCR values follow a similar 11-year cycle to the solar cycle; however, they vary only slowly with time unlike the solar cycle spectrum which is susceptible to bursts of activity and changes in environment.

2.2.1 Aircrew Exposure to GCR

Under the recommendations of the International Commission on Radiological Protection in Publication 60 [29], the European Union revised their radiation safety standards to include cosmic radiation as part of the occupational exposure of their staff. In 2004, Bartlett et al. analyzed cosmic radiation exposure to aircrew as well as means of protection with a focus on the safety changes in the European Union. In the United Kingdom, around 15% of the total annual dose from natural sources of radiation is by cause of cosmic radiation. Additionally, the level to which dose rate increases with increasing altitude is dependent on latitudinal location. For example, at temperate zone latitudes the effective dose rate at an altitude of 8 km is around 3 μSv/h; however, near the equator the dose rate decreases to around 1-1.5 μSv/h at the same altitude [6]. It comes as no surprise that in the United Kingdom, because of its relatively high latitude, aircrew receive one the highest annual doses of radiation among those occupationally exposed.

Bartlett et al. concluded that depending on altitude, duration of flights, and annual dose, aircrew should proceed differently to assure their own safety. Crew members flying at altitudes higher than 15 km should carry active radiation monitors to detect significant variations in radiation levels. Crew members receiving an annual effective dose from 1 mSv to 6 mSv should use computer prediction codes to record their intake of radiation. This should assure that no crew member exceeds the recommended 6 mSv effective dose. Finally, for crew members whose annual dose is below 1 mSv no action is necessary. These values for effective dose intake vary with flight paths as well as flying hours. For example, 200 hours of flying at 10.7 km in temperate latitudes would equate to the same dose, less than 1 mSv, as 400 hours at the same altitude near the equator.

2.3 CARI-7A

The Civil Aviation Research Institute (CARI) software was created by the FAA to calculate doses of ionizing radiation stemming from GCR in the Earth's atmosphere [20]. Different versions of CARI have been developed since its emergence in the 1980s with the latest being -7 and -7A, both offering the most up-to-date and accurate calculations of particle flux and dose. CARI-7A answers two major questions independently: what cosmic radiations are interacting with the atmosphere at a specific day and time and what dose rate corresponds to this interaction [30].

The creators of CARI-7A first utilized MCNPX 2.7.0 to calculate a database of atmospheric particle spectra from isotropically incident primary GCR particles [20]. CARI-7A uses this data base to predict the GCR fluence for past and future conditions. Additionally, CARI-7A uses two of the best modern models based on National Aeronautics and Space Administration (NASA) evaluations on GCR: the International Standards Organization 15390:2004 (ISO) model and the Badhwar and O'Neill 2011 (BO11) [31] and 2014 (BO14) [32] models. Both models provide the GCR spectrum at the Earth's orbit; however, they differ on their handling of the effects of transport through the heliosphere to the Earth's magnetic field [20] [33]. With the Badhwar and O'Neill models these effects are handled within the models while the ISO model use heliocentric potentials or those defined by the International Standards Organization, meaning that each model retains their own local interstellar GCR spectrum and solar modulation [20]. Additionally, Forbush decreases, the sudden decrease of galactic cosmic rays by 3%–20% for periods of minutes to hours followed by a gradual recovery to the previous intensity [7], and other variations in solar activity are handled as proposed by Lantos in the ISO model [34]. Although there is currently an updated Badhwar-O'Neill model (BO20) [35], the current version of CARI-7A does not use this version. Additional information on the Badhwar-O'Neill

models employed by CARI-7A are found in O'Neill's papers [31] [32].

The main menu for CARI-7A is shown in Fig. 2. This program assumes an adult on a nonstop flight, disregarding position within the aircraft as well as type of aircraft, to calculate dose rate with an altitude limit of 100 km and a travel date after January 1958. CARI-7A can intake a user-specified flight path using a specific file format. The first line of the file will represent the flight date, time (optional), and name. The second line will represent the headers labeled "DEG" (integer degrees latitude), "MIN" (real minutes latitude), "N/S" [North or South designator (equator can be either)], "DEG" (integer degrees longitude), "MIN" (real minutes latitude), "E/W" [East or West designator (prime meridian can be either)], "FEET" (integer altitude in feet), and "TIME (MIN)" (integer time in minutes from start of flights). The following lines will represent the waypoints where the data within each point is comma separated. The latitudinal and longitudinal position are represented in units of degrees (integer degrees) minutes (real minutes) which are unit equivalent to decimal degree units.

Within its capabilities, CARI-7A can output atmospheric particle fluence, effective dose based on International Commission on Radiological Protection (ICRP) Publication 60 and 103 recommendations [29] [36], ambient dose equivalent ($H^*(10)$), and whole-body absorbed dose [20]. Within the atmospheric particle fluence and any of the dose outputs, CARI-7A gives these values either as a total or as the partial contribution from a specific particle (37 particles available [37]). Finally, although the program considers the solar activity and the geomagnetic fields for its GCR rates, CARI-7A is unable to calculate solar particle events within its dose results.

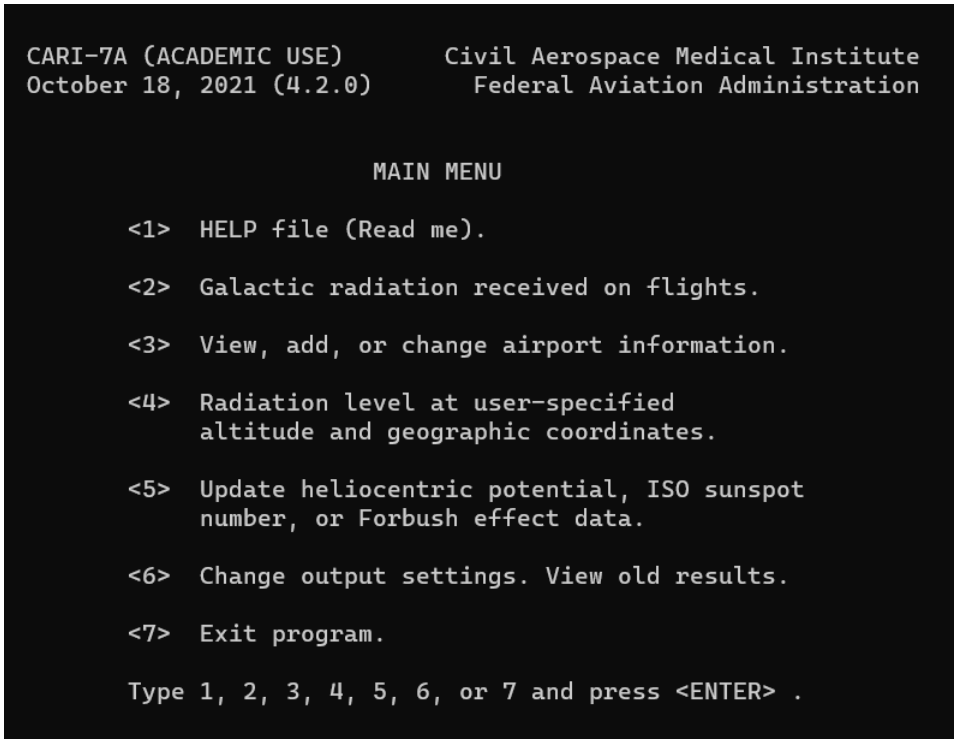

Figure 2: CARI-7A executable file main menu with all possible choices for outputs.

2.3.1 Comparison of GCR Models

In 2012, the European Radiation Dosimetry Group published a paper comparing several codes assessing radiation exposure of aircraft crew exclusively from GCR [4]. Some of the codes are used routinely for radiation protection purposes while others are purely for scientific use. Dose assessment of aircraft crew requires the calculation of effective dose given by

$$E = \sum_T w_T H_T = \sum_T w_T \sum_R w_R D_{T,R}, \tag{1}$$

where w_T is the tissue weighting factor and H_T is the dose dependent on a certain tissue (equivalent dose). H_T is also measured by the sum of the product of the radiation factor, w_R, and the mean absorbed dose, D, from radiation, R, in the tissue, T [4]. The weighting factors for both radiation and tissue are defined by the

International Commission on Radiological Protection. Effective dose is a derived and not a measurable quantity, therefore it should only be used for setting and verifying radiation limits for the purpose of protection [38]. On the other hand, operational radiation protection, specifically area monitoring at flight altitudes, uses ambient dose equivalent, $H^*(10)$. In this context, equivalent dose is found with

$$H = QD, \tag{2}$$

where Q is the biological effectiveness of radiation and D is the absorbed dose at a point of interest [4]. Specifically, for $H^*(10)$ the point of interest is 10 mm from the radiation source. For the purposes of this paper, the authors solely test codes with the ability to output ambient dose equivalent (or its rate). This project aims to compare the level of consensus between codes routinely used for radiation protection, therefore the authors choose to provide the results from this study anonymously meaning none of the results will be attributed to a specific code. Within their analysis, the authors chose 23 representative flights at a variety of latitudes. Additionally, within the 23 flight they chose six flights which had a duration of more than 13 hours, broadening the span of this research.

One of the codes they used that was of particular interest for this project was CARI, in this case CARI-6M which was the latest version at the time of this paper. CARI can give an estimate of the whole-body absorbed dose using National Council on Radiation Protection (NCRP) Report 116 [39] radiation weighting factors and effective dose using ICRP Pub. 60 radiation weighting factors. This specific report released the results in an anonymous manner, meaning we are unable to tell which codes gave what dose and dose rate values. However, they concluded that the overall agreement was better than 20% from the median. For flights at 37,000 ft (11.3 km) all dose rate results were within $\pm$ 1 μSv/h. The authors found greater spreads in dose

rate results, close to 50%, for flights closer to the equator compared to flights close to the poles, with a spread close to 20%. Additionally, the dose rate values from a flight close to the equator flying during solar maximum conditions matched closely to the same flight flying during solar minimum conditions, with no exact value provided by the research document. On the other hand, the dose rate values from a flight close to the poles flying during solar maximum conditions were 50% higher than those from the same flight flying during solar minimum conditions.

2.3.2 Model Validation

The Community Coordinated Modeling Center (CCMC) invited the FAA, the German Aerospace Center (DLR), and NASA to share their galactic cosmic ray models [CARI-7A (FAA), PANDOCA (DLR) and NAIRAS (NASA)] on their web page to further inform users on the uncertainty of their results as well as provide feedback to the creators of each model. The study intended to validate these models with measurements of the omnipresent radiation field created by GCR under an undisturbed magnetosphere [18]. Although this type of data does not consist of reliable measurements during severe space weather events, this is the first step towards complete validation of these predictive models.

This experiment used 10 total flight dates and positions, six to measure ambient dose rate equivalent, $dH^*(10)/dt$, and four to measure absorbed dose rate in silicon, dD_{Si}/dt. The data consisted of dates during the transition period from solar cycle 23 to solar cycle 24 (6-7 November 2007), i.e. a solar minimum, and close to the solar maximum during solar cycle 24 (14-15 May 2013) all during quiet space weather conditions. Additionally, the range in latitudes and longitudes encompassed 48.3 N to 60.1 N and 8.7 E to 10.3 E respectively. Finally, the flight levels varied between 320 and 400, signifying 32000 and 40000 feet in altitude respectively. Additional details

of this data are found in Meier's paper [18].

Within the project methods, Meier et al. decided to compare the values of ambient dose rate equivalent and absorbed dose rate in silicon given by the models, d^{model}, based on its relative deviation, Δ, from the measured quantities, d^{meas}:

$$\Delta = \frac{d^{model} - d^{meas}}{d^{meas}} [18]. \tag{3}$$

From the six flights used to compare average ambient dose rate equivalent, CARI-7A outputs had a relative deviation from the measured value of -8% to 6%, PANDOCA -6% to 14%, and NAIRAS -21% to 52%. From the four flights used to compare average absorbed dose rate in silicon, CARI-7A outputs had a relative deviation from the measured value of 0% to 11%, PANDOCA -11% to 9%, and NAIRAS -13% to 35%. The mean deviation of the relative deviation for ambient dose rate equivalent and absorbed dose rate in silicon for CARI-7A was 6% and 8%, PANDOCA 7% and 7%, and NAIRAS 23% and 23% respectively. These results are encouraging for the use of CARI-7A as an accurate model to output the radiation effects of GCR.

2.4 Solar Particle Events

Solar particle events consist of accelerated particles released by the Sun. This phenomenon involving the Sun's capability of producing large bursts of radiation has been studied since late 1950s. Research was sparked after the solar cosmic-ray event of February 1956; previously, there have only been four events measured with ground level detectors [40]. While the composition of SPE varies from event to event, on average the composition is 96% protons, 4% alphas and a small fraction constitute highly charged, highly energetic ions. These percentages closely resemble those within GCR; however, SPE differ in their acceleration energy and sporadic nature. Compared

to GCR, particles from SPE are accelerated at lower energies (between 10^6 and 10^{10} eV) and are therefore only a radiation concern at higher altitudes and latitudes [16]. For this reason, most of the research surrounding this topic is focused on space travel and safety of space equipment, not on basic aircraft flights and personnel.

Although generally SPE occur during times of solar maximum, the correlation between both phenomena does not always exist, unlike the relationship of the solar cycle to GCR. Additionally, even within a solar particle event the intensity and energy spectrum of each event can vary throughout its duration of a few hours to several days. The intensity of an event in this case is described as the number of ions per unit area with energy greater than a certain threshold of penetration. While large SPE are less frequent than smaller ones, one of these highly energetic events can deposit a flow of protons with energies larger than 30 MeV within the duration of several hours or days. At these energy levels, protons are strong enough to penetrate EVA spacesuits which is often used as a threshold for SPE [8]. The lack of predictability makes SPE a dangerous phenomenon for aircrew since just one unprecedented large event could significantly increase the annual dose intake for a crew member. In general, this type of ionizing radiation reaches the Earth's atmosphere isotropically; however, for higher energy particles, data has shown a preferred direction 30° to 60° west of the Earth-Sun line [40]. For lower energy particles the generalization still stands of isotropic behavior near the surface of the Earth.

2.4.1 Aircrew Exposure to SPE

In 2014, the National Institute for Occupational Safety and Health (NIOSH) performed studies detailing the potentiation effects on flight attendants' reproductive health under the influence of previous work evaluating the increased risk of this career field. Anderson et al. assessed the radiation dose exposure purely from SPE at

commercial aviation altitudes to combine SPE exposure with GCR dose estimates [16]. The research consisted of gathering the flight history records of 2174 flight attendants ages 18 to 45 during two separate study periods, 1992 to 1996 and 1999 to 2001. Additionally, solar storm data was obtained from the National Oceanic and Atmospheric Administration (NOAA) Space Weather Prediction Center during the respective study periods. To estimate the radiation dose solely from SPE, Anderson utilized the Nowcast of Atmospheric Ionizing Radiation for Aviation Safety (NAIRAS) model. This computational tool provides scientists with real-time predictions of ionizing radiation dose rates (SPE and GCR included) at commercial aviation altitudes [41]. Furthermore, radiation dose solely from GCR was estimated using CARI-6P computer program (a previous version of CARI-7A). The following equation was used to calculate and estimate the radiation dose solely resulting from expose to SPE, D_{SPE}, for a generic flight with a specific origin and destination, and at a specific date:

$$D_{SPE} = D_{CARI} \times \frac{1}{2}\left[\left(\frac{\dot{D}_{SPE}}{\dot{D}_{GCR}}\right)_{ori} + \left(\frac{\dot{D}_{SPE}}{\dot{D}_{GCR}}\right)_{des}\right], \tag{4}$$

where D_{CARI} represents the GCR dose calculated from CARI-6P, $\dot{D}_{SPE}$ represents the average SPE dose rate at origin, *ori*, or destination, *des*, calculated by NAIRAS, and $\dot{D}_{GCR}$ represents the average GCR dose rate at origin or destination calculated by NAIRAS. The authors did not provide further explanation for the use of this equation to isolate the dose from SPE.

This study found the absorbed (and effective) flight segment doses averaged 6.5 μGy (18 μSv) and 3.1 μGy (8.3 μSv) for study period A and B, respectively [16]. The maximum dose was 445 μGy (1.243 mSv) and 20 flight segments had doses higher than 190 μGy (0.5 mSv), the monthly limit recommended by the National Council on Radiation Protection and Measurements for pregnant aviators. Additional details of

these results are found in Anderson's paper [16]. During a solar particle event flight attendants could be exposed to significant doses of ionizing radiation which could endanger them or, if pregnant, their fetus.

2.5 SIRE2

In August 2016, Fifth Gait Technologies released the Space Ionizing Radiation Environment and Effects (SIRE2) toolkit to serve as a facilitator for space radiation environment calculations, specifically building upon previous models such as the Cosmic Ray Effects on Microelectronics (CREME) tool [21]. SIRE2 was originally designed as a toolkit for mission planning of space vehicles, extending the radiation environment to satellite orbits and arbitrary trajectories of spacecraft [21]. Although my project is focused on military aircraft and not spacecraft, the software can still be utilized as a means of calculating SPE ionizing radiation within the scheme of the problem. SIRE2 can take in specific trajectory tracks at various altitudes and still provide an estimated flux value for SPE for the duration of the flight. Because SPE are mostly an issue in space environments, most of the tools available are designed for this type of environment.

This toolbox offers three methods for calculating geomagnetic transmissions: the CREME-96, the Smart-Shea 2005, and the Smart-Shea 2022 models. The CREME-96 model is based on the October 1989 solar particle event, one of the strongest storms in recent years. The Smart-Shea 2005 and Smart-Shea 2022 allow the user to specify their own global geomagnetic storm index; Smart-Shea 2005 uses the Planetary K-index (Kp) while Smart-Shea 2022 uses a combination of the Planetary K-index and Disturbance Storm Time index (Dst). Both of these values characterize the magnitude of geomagnetic storms. More information on the specific values of both indices is found in the SIRE2 User Guide [42].

SIRE2 offers a graphical user interface (GUI), shown in Fig. 3, to work through all the models and tools under a single screen, facilitating the use of this toolkit. Within the program SIRE2 can intake a user-specified flight path using a specific file format, different from CARI-7A, called STK. The first line of this file will represent the headers labeled "Time (UTCG)" (time stamp with date and time), "Lat (deg)" (latitude in decimal degrees), "Lon (deg)" (longitude in decimal degrees), "Alt (km)" (altitude in kilometers), "Lat Rate (deg/s)" (latitudinal rate), "Lon Rate (deg/s)" (longitudinal rate), and "Alt Rate (deg/s)" (altitude rate). The following lines fill in the waypoints for the flight path. The latitudinal, longitudinal, and altitude rate values are deemed unnecessary for the toolkit to run properly, therefore can simply be filled with a generic value such as 0.001.

To specify the interplanetary environment made up of solar energetic particles, the user can choose the average environment during the worst week, worst day, or peak flux of the October 1989 solar storm. Additionally, the user can also use the Mission-Specific Solar Radiation Environment Model which creates a design reference environment of solar energetic particle fluxes for a specific date, length of flight, and confidence level [42].

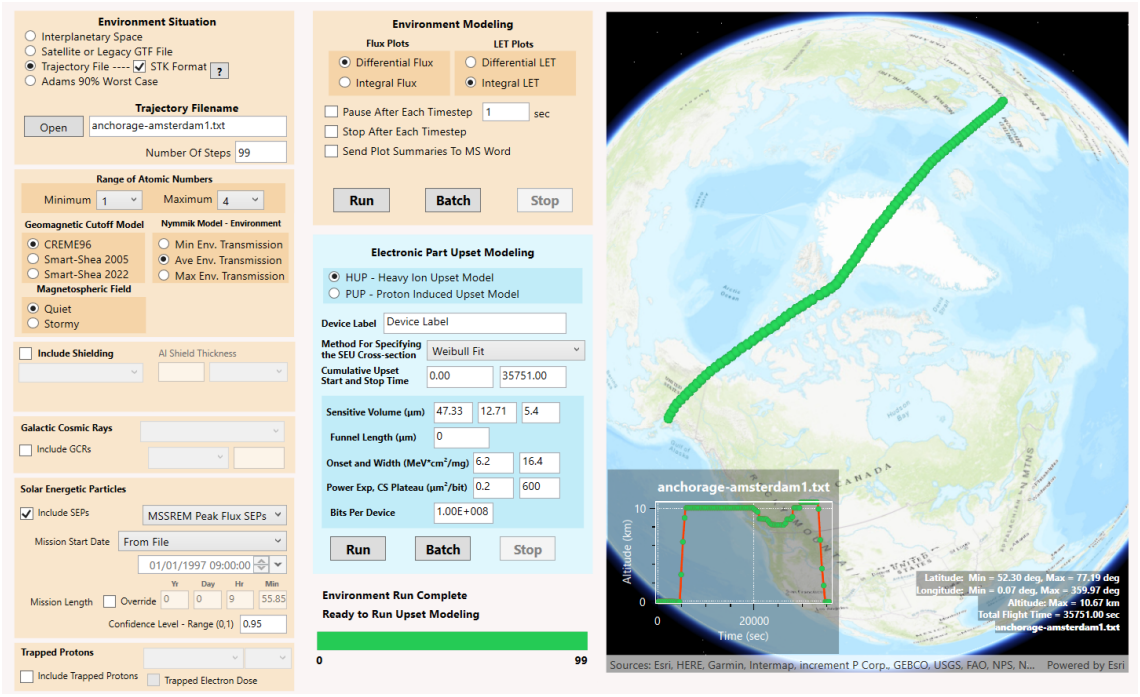

Figure 3: SIRE2's guided user interface after a completed run with the selected parameters listed on the left of the screen and the map depicting the route as well as where each individual timestep was taken (in green) on the right of the screen.

III. Methodology

3.1 Selection of Flight Tracks and Dates

With the available timeframe for this project, it was crucial to limit the number of flight tracks and dates I tested while maintaining a high level of variation to make comparative analysis at the end. To accomplish this, I simulated two separate fight paths, each running during two separate dates for a total of four different flights. I chose the flight paths to include a flight near the equator, from Singapore to Nadi, and a flight near the Arctic circle, from Chicago to Reykjavik. Instead of coming up with my own waypoints through the flight path, I employed FlightRadar24 [43]. I reasoned that while these flight paths might not resemble a real military flight mission, they would provide me with realistic altitudes, speeds, and rates of change of both values. FlightRadar24 is an open-source flight tracking service providing real-time and past information on commercial flights around the world. This site allows the user to choose an airport and view all the tracked flights from and to this location. Once the user has chosen a path, they can download a .csv file with all the waypoints through the specific flight. The file gives the time stamps, date and time of flight, callsign, positions (latitudinal and longitudinal), altitudes, speeds, and directions. Because I was unable to gather military flight data, for issues of classification and open-source availability, commercial flight data was used for this project. The flight path from Singapore Changi Airport to Nadi International Airport is shown in Fig. 4 and the flight path from Chicago O'Hare International Airport to Keflavik International Airport is shown in Fig. 5.

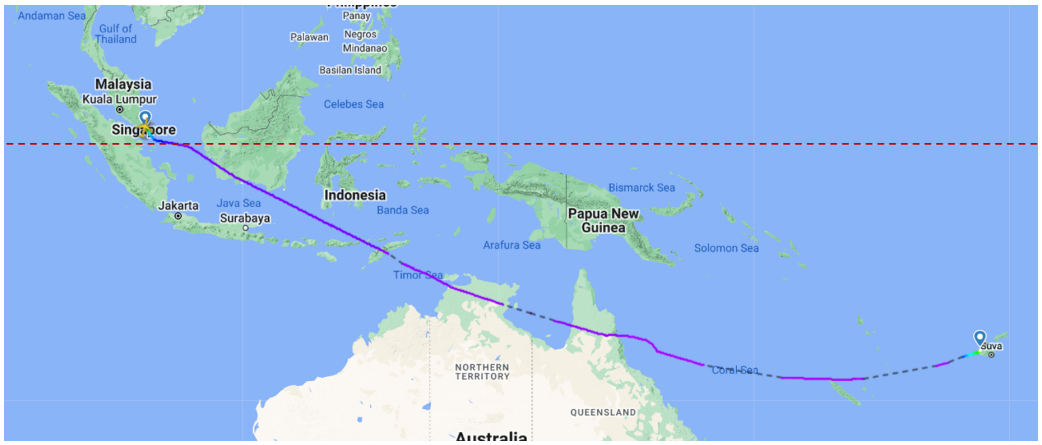

Figure 4: World map showing flight track from Singapore Changi Airport to Nadi International Airport as a blue circle and the Equator represented by red dashed horizontal line [43].

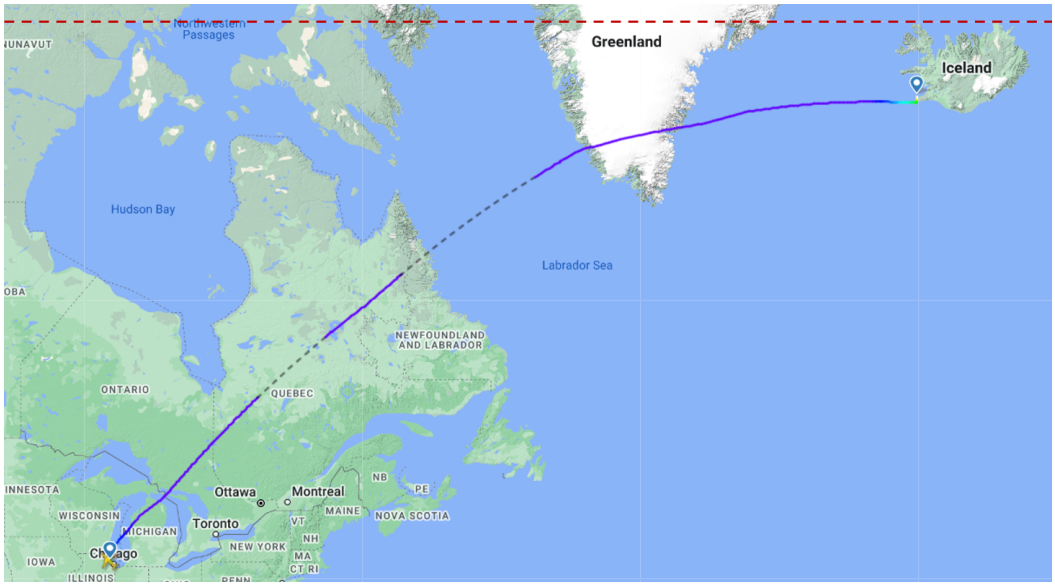

Figure 5: World map showing flight track from Chicago O'Hare International Airport to Keflavik International Airport in blue and the Arctic line represented by red dashed horizontal line [43].

Additionally, I chose the flight dates to cover a day during a solar minimum, January 1st 1997, and a day during a solar maximum, March 1st 2001. These dates correspond to the 23rd solar cycle lasting from May 1996 to January 2008. In choosing these specific flights I was able to compare the expected variation in dose values

through the flights, e.g. a higher GCR dose value during a solar minimum than a solar maximum, to those calculated at the end of this study. Because CARI-7A and SIRE2 both intake flight paths using different file formats from one another, I created a Python code to convert the flight path information from the .csv file with the selected dates to both CARI-7A and SIRE2 formats. Although these conversions could have been done by hand, utilizing Python saved time and left functions for others to correctly convert different flight paths in the future.

3.2 Use of CARI-7A for GCR Data

After creating the appropriate files to run CARI-7A, I utilized this software to collect the necessary particle flux information from GCR for each flight. Additionally, CARI-7A's calculated effective dose was output for each flight to use as a comparison later in the project. Unlike SIRE2, CARI-7A does not work through a GUI: instead it uses an executable file to execute commands directly. Through the executable file, CARI-7A gives the choice of obtaining the galactic radiation received on a specific flight or the radiation level at a specific altitude and geographic coordinate. The latter gives users the option of collecting galactic radiation data at a specific point in the atmosphere without needing a specified flight path with defined waypoints. Because the scope of this research focuses on the radiation received by aircrew for each specific flight, I used CARI-7A's first option.

CARI-7A gives the option of outputting the total fluence and effective dose for all GCR particles or the specific contribution to particle fluence and effective dose of each particle. I chose to output both the total effective dose for all particles and the specific contribution to secondary particle fluence of each particle. The effective dose output served as a comparison value to my own calculated effective dose later in the project, and the particle fluences served as the radiation sources I used as the

source term for the MCNP model of the aircraft. As described in 2.3, CARI-7A gives the user a list of particles to choose from. Instead of outputting the partial fluence contribution of all 37 particles available, I only chose the neutron, photon, electron, positron, negative muon, positive muon and proton fluences since those are the main particles contributing to galactic radiation found at flight-altitudes [6].

For both dose and particle fluence values, I selected the Badhwar and O'Neill 2014 model, since this model is a significant improvement to its previous version, the Badhwar and O'Neill 2011 [32]. Under the two choices for effective dose provided by CARI-7A, I selected the ICRP Pub. 60 recommendations instead of the ICRP Pub. 103 recommendations. Although ICRP Pub. 103 was released later than Pub. 60, MCNP can only conduct flux to dose calculations using Pub. 60 and not Pub. 103. Because I will compare between my calculated dose through MCNP and the CARI-7A output, I need to use the same weighting factors for both values. Running CARI-7A resulted in an effective dose value in units of μSv and particle fluences in units of particle per square centimeter.

3.3 Use of SIRE2 for SPE Data

I used the SIRE2 files previously created and collected the necessary particle flux information from SPE for each flight. Unlike CARI-7A, this software is unable to calculate an effective dose for each flight; however, SIRE2 does give an absorbed dose output in units of rads. To use this value for a comparison between the software and my own model, I calculated the equivalent dose using Eq. 1 where the tissue weighting factor is equal to one (since I am measuring whole body dose) and the radiation factors are taken from the ICRP Pub. 60. According to this publication, the radiation factor for protons is equal to two and for alphas this value is equal to 20 [29].

Using SIRE2's GUI, I configured the software to output the desired values. First, I increased the number of steps from the default 20 to the maximum amount 99. Increasing the timesteps allows the model to make more calculations throughout the run. I also limited the range of atomic numbers to only include protons and alphas, as on average both compose the majority of the particles in SPE. For the geomagnetic cutoff model, I chose the CREME96 instead of manually entering my own Kp index values through the Smart-Shea models. Because I do not have data on the Kp index values during the time or date of each flight, I thought proceeding with the CREME96 model under an average environment transmission would give me the best results.

For the solar energetic particle fluxes, I chose the Mission-Specific Solar Radiation Environment Model using the specific flight date. This model designs a reference environment of solar energetic particle fluxes for my flight path instead of just using the average environment during the worst week, worst day, or peak flux of the October 1989 solar particle event. Because one of the dates corresponds to a solar minimum, having solar energy particles that only reflect a storm event would not properly model my environment. After running the program under these parameters, I used the environment and dose plots to output Excel files obtaining the free-field particle fluence values, in units of particle per square centimeter, and the free-field total dose values, in units of rads, through the 99 timesteps.

3.4 Development of MCNP Input Decks in SWORD

The necessary MCNP input decks used throughout this project were first created using SWORD, specifically with the aid of its geometry builder viewer. MCNP is a particle transport code developed by Los Alamos National Laboratory [44] Within MCNP the user can model particle transport through a user specified three-dimensional geometry with defined materials and surface dimensions. SWORD simplifies the ge-

ometry building aspect of MCNP through its CAD-like graphical user interface [45]. Using SWORD the user can add simple or complex objects into their environment, and adjust properties such as size, material, shape, position and radioactive emission of said objects. Within SWORD's library of objects, the software has pre-built geometries for several items including a Boeing 737 airliner with pilot, copilot, cargo compartments and 124 passengers, an A-10 Thunderbolt II close support aircraft without the main cannon or pilot, and a Cessna Skycatcher light plane with pilot and copilot. In addition to their geometric configuration, these library items have pre-selected material properties closely matching the true material configuration of the real item. For example, although humans are made of water, fats, proteins, minerals and carbohydrates, the pilots, copilots and passengers within SWORD are solely composed of water. Because of the project's focus on military aircrew, I decided only to use the A-10 and the Boeing 737 aircraft since both planes, and their variations, have been or are currently in the Air Force's stockpile. Additionally, both aircraft serve as examples, size and utility wise, of fighter aircraft and tanker/cargo aircraft. It is important to note that this project is solely focusing on atmospheric ionizing radiation and not any other type of radiation that might be emitted by the electronics within an aircraft, for example non-ionizing radiation. For this reason even though SWORD does not provide the geometry for the electronics normally found inside each aircraft, it does not make a difference to my final dose calculations.

Starting with the A-10 input deck, I added the aircraft to a new SWORD environment. Unlike the Cessna or Boeing 737, this aircraft did not have a pilot within its cockpit as shown in Fig. 6. Although SWORD also has a person within its object library, this person is standing up which would present a geometry issue within MCNP as seen in Fig. 7. The overlapping geometry of the legs on the person going through the A-10 pilot seat is not allowed in MCNP. Additionally, while the user can

rearrange the position of any object using SWORD, there is no configuration that would keep the "pilot" away from any other surface within the plane.

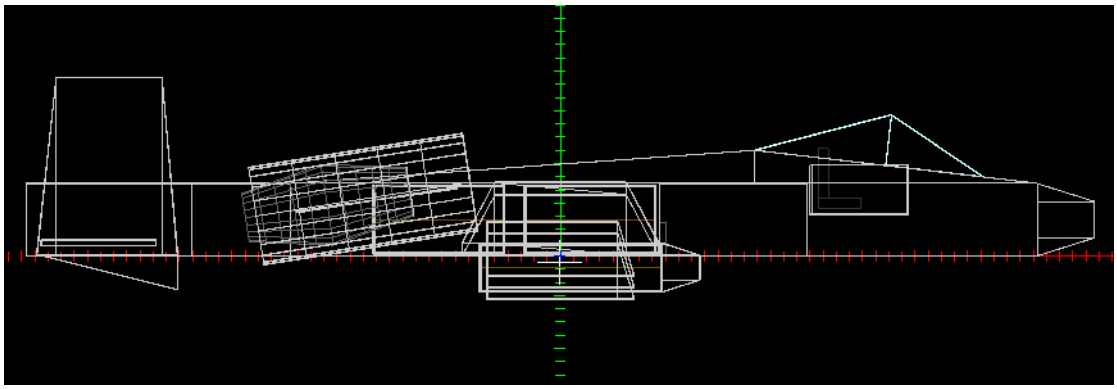

Figure 6: Side view from SWORD's geometry viewer of the original A-10 Thunderbolt II object. The aircraft has a wingspan of 1753 cm, a height of 447 cm, and a length of 1630 cm.

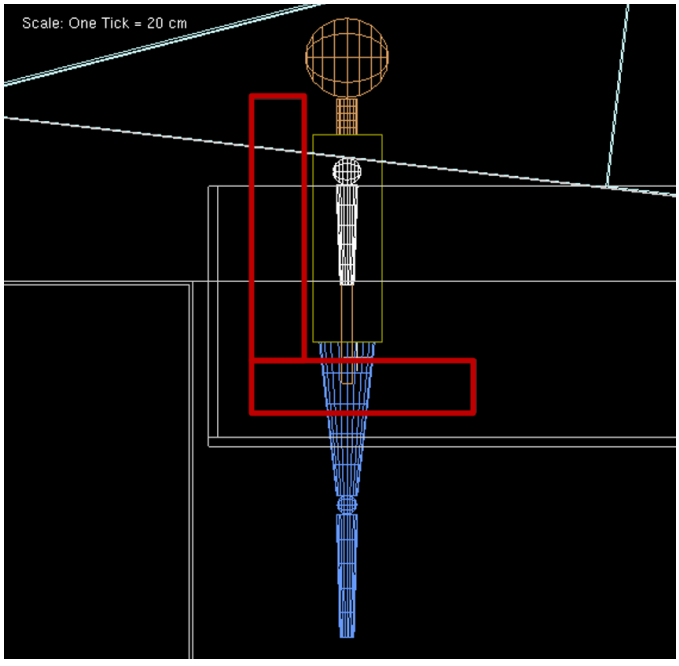

Figure 7: Side view from SWORD's geometry viewer of a standing person within the A-10 cockpit showing that the legs of the pilot, in the current position, go through the seat of the plane.

Within the available options, I considered adding a cylinder of water in place of a person to ensure that no errors in geometry would arise. This object could be of the

same mass and material as a person in SWORD; however, I would lose the true shape and distribution within the cockpit of the pilot. Instead of this option I opted to use the pilot already embedded within the Cessna plane and add it to my original A-10 since this person is in a seated position. This process required deleting every other object within the Cessna geometry leaving just the pilot at the end. I could have used a pilot or passenger from the Boeing 737 airframe since they are also in a seated position; however, singling out a person from this plane would have required tedious amounts of work since this aircraft has far more objects within its geometry than the Cessna airframe. After isolating the pilot from the Cessna aircraft, I embedded the person inside of the A-10 cockpit, positioning them on top of the seat assuring no issues with the geometry as shown in Fig. 8.

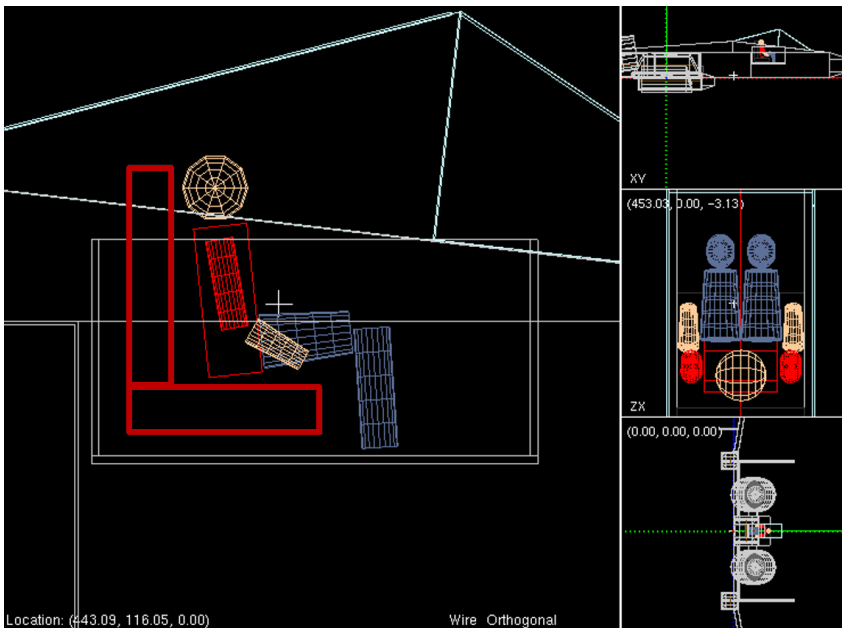

Figure 8: Side, top, and back view from SWORD's geometry viewer of a seated Cessna pilot within the A-10 cockpit showing from all angles that the person is not interfering with the plane's geometry, specifically the seat.

With SWORD the user can construct any type of radiation source as well as set detectors and MCNP tallies to any object within its environment, finalizing the input

deck. I used SWORD to set the MCNP cell, surface, and material data cards since the geometry viewer and library of objects within the software facilitates this process. The output control, physics, source, and tally data cards were added and modified afterwards to ensure the correct inputs were in place. Once I finished the geometry changes, I ran SWORD to output a text file with the designed MCNP input deck. Next, I constructed the Boeing 737 input deck using similar steps from before apart from adding a person since the Boeing 737 aircraft already included a pilot, copilot, and passengers as depicted in Fig. 9.

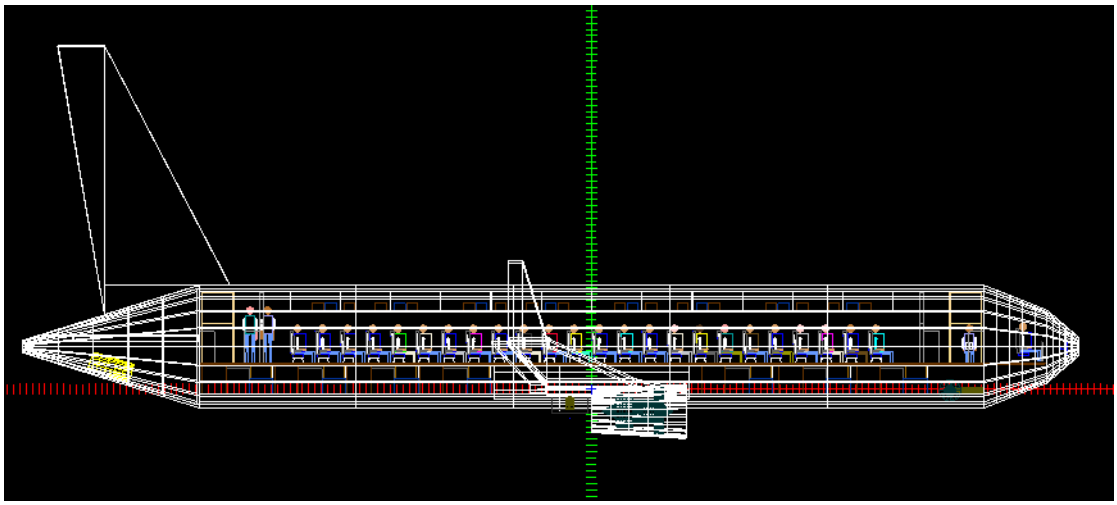

Figure 9: Side view from SWORD's geometry viewer of original Boeing 737 airliner object. The aircraft has a wingspan of 3680 cm, a height of 1277 cm, and a length of 3360 cm.

3.5 Development of the MCNP Radiation Source

Although CARI-7A outputs specific GCR particle fluences for each flight, the software is unable to output an energy spectrum for these particles. The creators are currently working on a similar program that can output the secondary particle spectrum; however, it is currently unavailable to the public. To minimize the run-times and work around this issue I constructed my radiation sources within MCNP generically. This means that I created seven different MCNP input files per aircraft

all with an energy of 1 MeV corresponding to each particle of interest: neutrons, photons, electrons/positrons, negative muons, positive muons, protons, and alphas. Because electrons and positrons are treated as the same particle within MCNP, there was no use in creating a separate input deck for each one. Although assuming that all the particles carry an energy of 1 MeV increases the uncertainty of my results, considering the details of the energy spectrum was beyond the scope of this project.

For the shape and type of each radiation source, I chose an isotropic source emanating from a spherical surface encapsulating each aircraft. Within the surface data card created by SWORD, there is already a box containing each plane and all its components. Instead of creating an entirely new surface and facing the challenges that come with changing the geometry within MCNP, I just changed the shape of the box to a sphere with a radius covering each aircraft completely. For the A-10 input decks I centered the sphere directly in the middle of the environment with coordinates (0,0,0) and a radius of 900 cm, as shown in Fig. 10. The surface data card reads

```
2 SPH 0 0 0 900
```

where the first number `2` represents the surface label number, `SPH` identifies the sphere shape, `0 0 0` are the coordinates within the environment, and `900` represents the radius in units of centimeters.

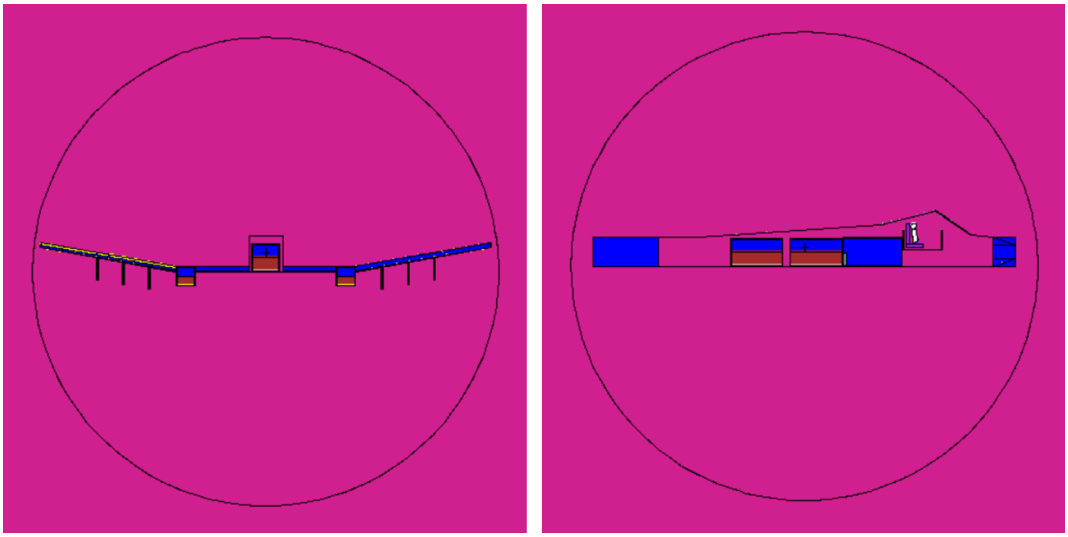

Figure 10: Front and side view from MCNP's plot viewer of A-10 aircraft surrounded by a spherical source.

For the Boeing 737 input decks, as shown in Fig. 11, I centered the sphere with coordinates (-150, 200,0) with a radius of 1900 cm. The surface data card reads

```
2 SPH -150 200 0 1900
```

with the values representing the same as those above for the A-10 surface data card.

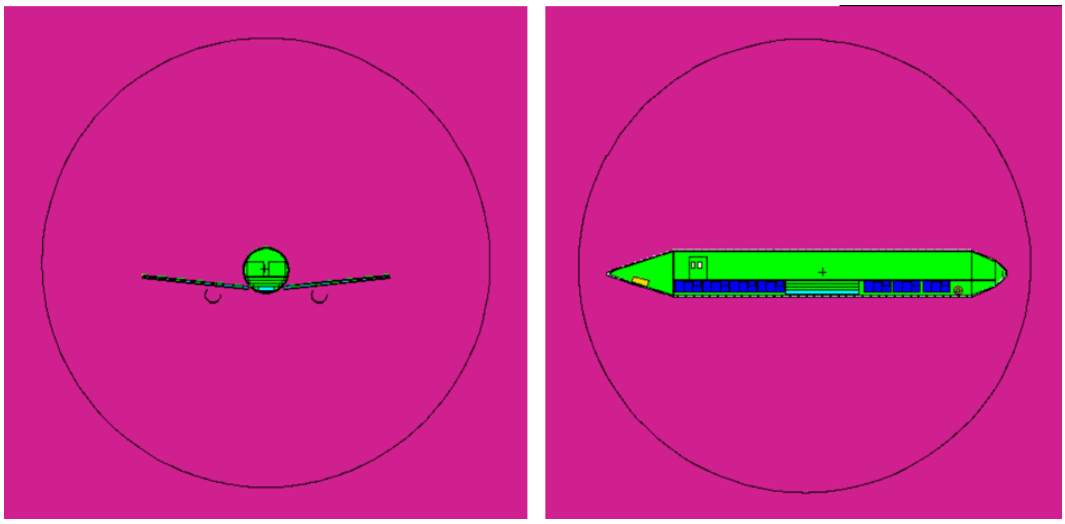

Figure 11: Front and side view from MCNP's plot viewer of Boeing 737 aircraft surrounded by spherical source.

Additionally, to create a more realistic environment, I changed the material of

this sphere to a vacuum under the cell data card. The particle fluence gathered from CARI-7A and SIRE2 both describe this value at an object. If the material of the sphere was air then there would be an extra gap of atmospheric material that the source would have to transverse before reaching the object, in this case the aircraft. This would not only add to the runtime but would give a wrong value of particle fluence reaching the surface of the plane. The source data card reads

```
SDEF PAR=N SUR=2 NRM=-1 ERG=1
```

with `SDEF` initiating the general source definition, `PAR` signaling the particle time (in this case neutrons), `SUR=2` representing the surface the source will emanate, `NRM=-1` representing the source emanating inwards, and `ERG=1` gives the energy of the source at 1 MeV.

Each individual input card for a specific source particle has a different MCNP physics data card. Within this section, I changed the particle `MODE` to only include the particles of importance for each source type. Although I could have kept a uniform particle `MODE` throughout all the source types, meaning they would all include every particle available on MCNP, that would significantly increase the runtime. As a proof of concept I ran shorter runs through MCNP for all source types with all particles included under `MODE`. I found that only certain particles proved important for each source. Therefore, for the neutron sources I included neutrons, photons and electrons; for the photon and electron sources I included both photons and electrons; for the negative muon sources I included electrons and negative muons; for the positive muon sources I included electrons and positive muons; for the proton sources I only included protons; and for the alpha sources I only included alphas.

3.6 Development of the Material Data Card, MCNP Tallies and Stopping Parameters

MCNP requires material specifications for all of its surfaces and cells under this configuration: `ZZZAAA` where `ZZZ` represents the material's atomic number and `AAA` represents the material's atomic mass number [46]. When SWORD outputs its input decks, its material data cards only call for the element of the material, meaning that within its integer value of the material only the atomic number is included without the atomic mass number (`ZZZ000`). Although this configuration works for photon particle transport within MCNP, neutrons need the atomic mass number identifier. For this reason I changed each input deck to contain the necessary atomic mass number identifier using the Compendium of Material Composition Data for Radiation Transport Modeling [47].

The purpose of this project is to calculate the final effective dose received by the aircrew inside of an aircraft solely from ionizing radiation. MCNP gives the user the ability to either enter a point wise response, e.g. a flux-to-dose conversion factor, as a function of energy to modify a regular tally or apply built-in conversion functions provided by the software through `DE` or `DF` cards. This means, for example, that instead of outputting the flux per source particle received by the passengers within the aircraft and then having to convert this value to dose, MCNP can calculate this value automatically. One of the standard default dose functions is the ICRP Pub 60 effective dose conversion function for energy deposition tallies. This function uses the particle's stopping power, $S(E, p)$ to create a multiplier of the absorbed dose. Stopping power is defined as the average energy dissipated by ionizing radiation in a medium per unit path length of travel through that specific medium [48]. The default function also uses a table for neutron quality factors, Q, and other particles

the following function is used:

$$Q_{ICRP-60}(S(E,p)) = \begin{cases} 0 < S(E,p) \leq 10, & Q_{ICRP-60} = 1 \\ 10 < S(E,p) \leq 100, & Q_{ICRP-60} = 0.32 * S(E,p) - 2.2 \\ 100 > S(E,p), & Q_{ICRP-60} = \frac{300}{\sqrt{S(E,p)}} \end{cases} \quad (5)$$

where the stopping power is in units of keV/μm [46]. The necessary `DF` card to use this function reads:

```
DFn IC=99 IU=1 FAC=-3
```

where `IC=99` calls for a specific dose conversion function in this case the ICRP-60 effective dose conversion function for energy deposition tallies. Additionally, `n` refers to the specific tally number identifier and `IU=-3` represents the final units for this conversion, rem per hour per source particle, required if using `IC=99`. This function works as an energy deposition-to-dose rate conversion meaning after all the runs I can very easily use the duration of each flight to scale up to the final effective dose value. Even though MCNP offers several other dose functions to choose from, such as the ICRP Pub. 21 or the ICRP Pub. 74 ambient dose equivalent, these only take into account neutron or photon dose. This means that the dose from a muon, proton or alpha, particles present in the sources for my project, would not be accounted for in these calculations.

To use this dose conversion function I first had to select the appropriate energy deposition tally. MCNP's designated energy deposition tally is `F6` with an output unit of MeV per gram per source particle. This specific tally takes the heating number from available nuclear data tables to find the energy deposition for neutrons, photons, electrons, and protons. The heating number refers to the energy deposited by the source particles during its collision path. For all other particles, the energy deposition

is found by adding the ionization energy, nuclear recoil, and energies of non-tracked secondary particles to a specific F6 collision estimator not explicitly stated or explained in the literature [46]. This tally requires the user to specify all secondary particles for each particle source in the MODE card. If a certain particle is not mentioned in the MODE yet appears it in the MCNP environment through a collision or by particle decay, the code assumes the particle's energy is fully deposited locally at the collision site. This means these non-tracked particles disappear from the environment and are unable to interact with other particles or material which is a poor assumption for those particles with high energy or materials with thin volumes [46].

With F6 the user has to specify each particle it wants a tally from meaning the output will show the dose rate of each individual secondary particle. Because I am only concerned with the total dose rate, I can use the collision heating tally, +F6 tally. With this card I can output the total energy deposition from all particles averaged over selected cells. For this project I needed to isolate the cells comprising the aircrew and turn them into detectors. For the A-10 configuration, I averaged the energy deposition across the different cells that make up the pilot (head, legs, torso, arms, etc.) by using the following +F6 tally and DF card:

```
+F16 208 209 210 211 212 213 214 215 216 217 T
DF16 IU=1 FAC=-3 IC=99.
```

The +F16 tally included all numbered cells and the T calls for an averaging of the energy deposition across the cells previously called. For the Boeing 737 input decks, there are several different people to choose from. Because I measured the dose from the pilot in the A-10 aircraft, I also made the pilot within the Boeing 737 a detector. Additionally, I wanted to test if there was a significant difference between the dose received by a pilot at the front of the plane in comparison to a passenger in the middle of the plane. To test this I choose a passenger sitting in row 12 on the window seat.

For reference, the Boeing 737 modeled by SWORD has 25 rows. In similar fashion to the A-10, I used the following +F6 tally and DF card for my Boeing 737 input decks:

```
+F16 (3134 3135 3136 3137 3138 3139 3140 3141 3142 3143 3144 3145 3146)
(683 686 689 692 695 698 701 704 707 710 713 716 719) T
DF16 IU=1 FAC=-3 IC=99.
```

The first grouping in the +F16 tally corresponds to the cells that encompass the pilot while the second grouping represents the passenger seating in row 12.

The output control data card informs MCNP of the specific conditions required to terminate the run. I set the stopping parameter corresponding to the total number of particles transported, NPS, so that each input deck would run for the same number of particles. Because the environment for the Boeing 737 was much larger than that of the A-10 (for reference the source sphere surrounding the Boeing 737 is 1,000 cm longer in radius than that of the A-10), I chose an NPS of 100,000,000 particles for the Boeing 737 input decks and an NPS of 50,000,000 for the A-10 input decks. I chose these numbers to minimize the run time of each input deck while still achieving a low error for the results. Additionally, I added the same random number generator, RAND, to each input deck to assure that any repeated runs done in the future would output the same value. I used the following line of code to implement my generator:

```
RAND GEN=2 SEED=133113311331133113
```

where GEN=2 represents the use of the L'Ecuyer 63-bit generator number 1 with a period of $9.2e18$ numbers and 133113311331133113 is the number generator seed for starting the transport of the first particle history in a run [46].

3.7 Final Dose Calculations

The three main pieces of data I gathered are: the particle fluence, in units of source particle per squared centimeter, corresponding to the GCR for each flight

path, the particle fluence, with the same units, from SPE for each flight path, and the corresponding effective dose rate per source particle received by each of my detectors, i.e. the pilots and passengers, from the generic particle sources. To convert these generic dose rates per source particle to effective doses for each specific flight path, I first converted the fluence values to number of source particles. The area unit in the denominator of fluence values represents the area of the modeled source from which the particles emit. The fluence value allows the user to scale up or down the number of particles depending on the size of the modeled environment. For the spherical sources the surface area of each is given by the following basic equation:

$$A = 4\pi r^2, \tag{6}$$

where r represents the radius of the source. For the A-10 and Boeing 737 input decks the surface areas were $1.01788e7$ and $4.53646e7$ squared centimeters, respectively. With this value I used the following equation:

$$\#\text{ source particles} = \text{fluence} \times \text{surface area} \tag{7}$$

to find how many GCR and SPE source particles are encountered by the aircraft after each flight in this modeled environment.

Afterwards I used the number of source particles and the length of each flight, in hours, to convert the dose rate per source particle to effective dose using the following formula:

$$E = \text{dose rate per source particle} \times \#\text{ source particles} \times \text{length of flight}. \tag{8}$$

The effective dose value from this calculation is in units of rem. For the final compar-

ison to the effective dose values calculated by CARI-7A and SIRE2 I had to convert rem to μSv by multiplying this value by 10,000. I accomplished all of these calculations using a Microsoft Excel spreadsheet to keep track of each flight and each aircraft value.

IV. Results and Analysis

4.1 GCR and SPE Particle Fluence Values

The first data set came from the particle fluence calculations of both CARI-7A and SIRE2. For GCR the program requires the user to go through each particle of interest separately for each flight and output its respective particle fluence. The final results are detailed in Table 1 rounded to the fourth significant digit in units of particles per square centimeter. Since CARI-7A does not include inherent uncertainty values for its results, I determined uncertainty in proportion to the last decimal of precision.

Table 1: Particle Fluence [#/sq. cm] Results from CARI-7A

Date	**Chicago-Reykjavik 01-01-97**	**Chicago-Reykjavik 03-01-01**	**Singapore-Nadi 01-01-97**	**Singapore-Nadi 03-01-01**
Neutrons	22.33 ± 0.01	15.08 ± 0.01	8.601 ± 0.001	7.845 ± 0.001
Photons	126.2 ± 0.1	106.8 ± 0.1	150.1 ± 0.1	142.8 ± 0.1
Electrons	4.208 ± 0.001	3.621 ± 0.001	5.344 ± 0.001	5.093 ± 0.001
Positrons	1.870 ± 0.001	1.610 ± 0.001	2.375 ± 0.001	2.264 ± 0.001
Neg Muons	0.3365 ± 0.0001	0.2846 ± 0.0001	0.3843 ± 0.0001	0.3604 ± 0.0001
Pos Muons	0.3365 ± 0.0001	0.2846 ± 0.0001	0.3843 ± 0.0001	0.3604 ± 0.0001
Protons	1.068 ± 0.001	0.7401 ± 0.0001	0.4730 ± 0.0001	0.4315 ± 0.0001

For SPE the process for acquiring respective particle fluences is less strenuous since the values for all particles of interest are provided in the same run. The final results are detailed in Table 2 also rounded to the fourth significant digit. Since SIRE2 does not include inherent uncertainty values for its results, I determined uncertainty in proportion to the last decimal of precision.

Table 2: Particle Fluence [#/sq. cm] Results from SIRE2

Date	**Chicago-Reykjavik 01-01-97**	**Chicago-Reykjavik 03-01-01**	**Singapore-Nadi 01-01-97**	**Singapore-Nadi 03-01-01**
Alphas	160,700 ± 1	26,120,000 ± 1	0.0	0.0
Protons	1,676,000 ± 1	132,600,000 ± 1	0.0	0.0

For the particle fluence values for GCR there is a clear pattern between the values during the solar maximum on March 1st of 2001 and during the solar minimum on January 1st 1997. There is always an increase in particle fluence between these two dates which is an expected pattern according to the literature. For the flights occurring near the North Pole, there is a higher relative increase in fluence and overall higher values compared to those experienced near the Equator. This behavior is expected since according to the literature the effects of GCR are felt greater near the poles (North or South). Additionally, the particle percentage breakup is not what was originally expected. The particle breakdown, according to the literature, consisted of mostly neutrons, followed by electrons and positrons, then protons and finally photons and muons. The number of photons in all four flights was higher than anticipated; however, the rest of the particles behaved as expected.

The results from SIRE2 were considerably less predictable than from CARI-7A. Although I was aware that there would be significant jump in particle fluence for the flight traveling near the North Pole, I was not expecting the magnitude of the end result. The proton particle fluences alone have values of a million to a hundred million times of what was found from GCR. The particle breakdown between alphas and protons follows the values found in literature; however, these values were far greater than any found in past research papers. Additionally, although I was expecting very

insignificant values for the particle fluences near the Equator, SIRE2's output of zero for both dates limited my analysis and my calculation of the impact of SPE during flight. For these reasons I am skeptical of the capabilities of SIRE2 in regards to commercial flight routes instead of satellite or space flight missions. For the rest of this chapter I will separate the effective dose values and other calculations between CARI-7A outputs and SIRE2 outputs.

4.2 MCNP Dose Rate Values

In total I had 14 different MCNP input decks to run. Depending on the source particle, there was a significant gap between run times. Neutron sources took around eight to nine hours while positive muons took anywhere from eight to ten days. Although MCNP6 has the ability to implement multi-threading for some of their input decks (those consisting only of neutrons, protons and/or electrons) the manner in which the input decks were constructed through SWORD limited my ability to use this feature for the six input decks to which this would have applied to. Every time I tried using this feature, I received a warning message telling me that MCNP6 would only be able to use one thread since the input deck did not meet the requirements for multi-threading. I presented my values rounded to the fourth significant digit in units of rem per hour per source particle. Additionally, unlike CARI-7A and SIRE2, MCNP6 releases each result with a respective relative error.

As shown in Table 3, except for the neutrons and photons, every dose rate per source particle value for the Boeing 737 was lower than that for the pilot inside the A-10. The geometry of the Boeing 737 is highly complex and filled with more objects of different material compared to the A-10 geometry. The pilot inside the A-10 aircraft is surrounded by a titanium aircraft armor (often referred to as a the bathtub) on the bottom half of their body and a glass cockpit on the top half, while the pilot

and passenger inside the Boeing 737 are completely surrounded by aluminum from the fuselage and fiberglass from the insulation covering the aircraft. The Boeing 737 object from SWORD does not include any glass for the passenger windows or the cockpit. All of these factors could account for the lower values in the Boeing 737 dose rates compared to the A-10. Additionally, the passenger in row 12 is surrounded by other passengers (made of water) and suitcases (made of cotton) above its seat, while the Boeing 737 pilot only has a co-pilot (made of water) to its right. This could account for the lower dose rates found in the passenger in row 12 compared to the pilot even though both are inside the same Boeing 737 aircraft. Because I am limiting the energy for each source particle to 1 MeV, having more material between the source and the detector decreases the number of particles that can reach the target. This could account for MCNP's zero values for the protons and alphas inside the Boeing 737. Initially, I hypothesized that these zero values could be related to the stopping parameter of 100,000,000 particles. From the several runs I performed prior to finalizing my methodology, I found that not providing enough particles to an environment significantly changed the end tally value. Therefore, I performed two extra runs for each particle source with a stopping parameter five and ten times the original value; however, these extra runs also gave zero values for the dose rates. It is important to notes that these dose rate values are independent of flight path and number of source particles. These MCNP output values only represent how many 1 MeV source particles reach the pilots and passenger per source particle.

Table 3: Dose Rates [rem/hr] per Source Particle Results from MCNP

Aircraft/ Detector	**A-10/ Pilot**	**Boeing 737/ Pilot**	**Boeing 737/ Row 12**
Neutrons	$7.371 \pm 0.040 \times 10^{-13}$	$3.158 \pm 0.024 \times 10^{-12}$	$1.180 \pm 0.014 \times 10^{-12}$
Photons	$3.042 \pm 0.020 \times 10^{-15}$	$8.753 \pm 0.071 \times 10^{-14}$	$4.624 \pm 0.047 \times 10^{-14}$
Electrons/ Positrons	$4.800 \pm 0.228 \times 10^{-15}$	$2.749 \pm 0.201 \times 10^{-16}$	$1.091 \pm 0.110 \times 10^{-16}$
Neg Muons	$2.137 \pm 0.033 \times 10^{-12}$	$9.950 \pm 0.151 \times 10^{-13}$	$3.753 \pm 0.092 \times 10^{-13}$
Pos Muons	$3.521 \pm 0.043 \times 10^{-12}$	$1.762 \pm 0.020 \times 10^{-12}$	$6.100 \pm 0.118 \times 10^{-13}$
Protons	$1.728 \pm 0.216 \times 10^{-14}$	0.0	0.0
Alphas	$2.446 \pm 0.306 \times 10^{-14}$	0.0	0.0

For the pilot inside the A-10 aircraft, the positive muons had the largest value for dose rate per source particle, making up 52.20% of the total dose rate value (as seen in Fig. 12). Coincidentally, the lowest value corresponded to the electrons/positrons, making up 0.07% of the total value. These values showed a significant gap between the highest and lowest dose rate per source particle output from MCNP. The particles with the highest influence in dose rates per source particle include the positive muons, the negative muons, and the neutrons. Even though these values are not specific to any particular flight path or date, meaning they are not taking into account the number of source particles encountered, they do clarify which particles have higher values of interaction, meaning more tallies, with the aircrew.

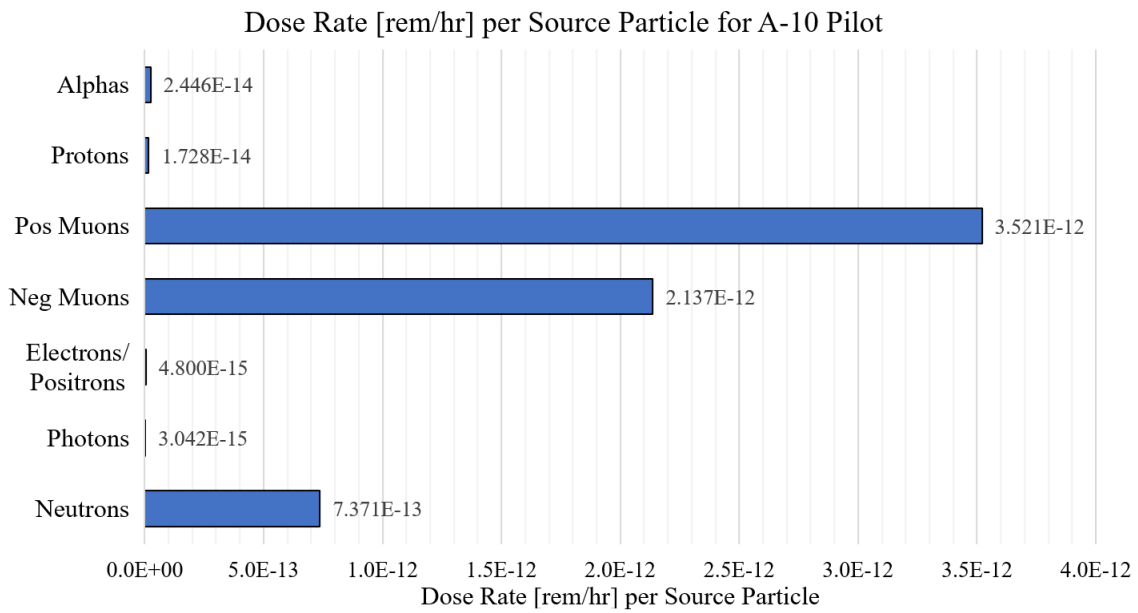

Figure 12: MCNP output of dose rate [rem/hr] per source particle for each type of source (neutrons, photons, electrons/positrons, negative muons, positive muons, protons, and alphas) corresponding to the pilot inside the A-10.

With the Boeing 737 configuration, both detectors followed the same pattern for highest and lowest value as seen in Fig. 13 and Fig. 14. Neutrons had the highest value while alphas and protons tied for last with a value of zero. Similarly to the A-10 geometry, positive muons, negative muons and neutrons made up majority of the dose rate values for the pilot and passenger. On the other hand, the difference between the highest value and the lowest value is not as great as with the A-10 pilot.

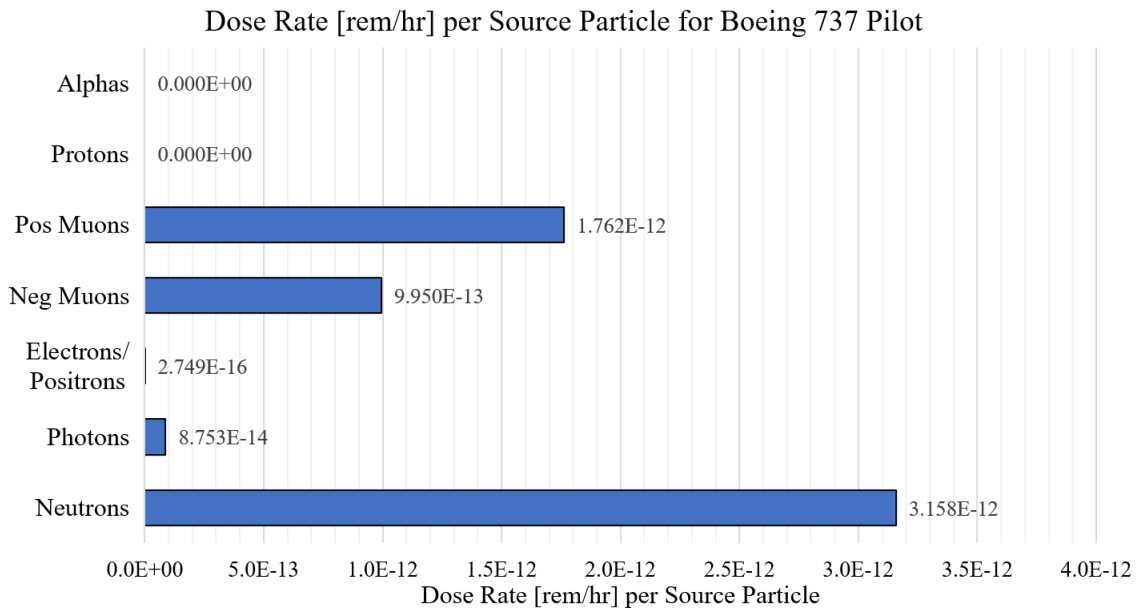

Figure 13: MCNP output of dose rate [rem/hr] per source particle for each type of source (neutrons, photons, electrons/positrons, negative muons, positive muons, protons, and alphas) corresponding to the pilot inside the Boeing 737.

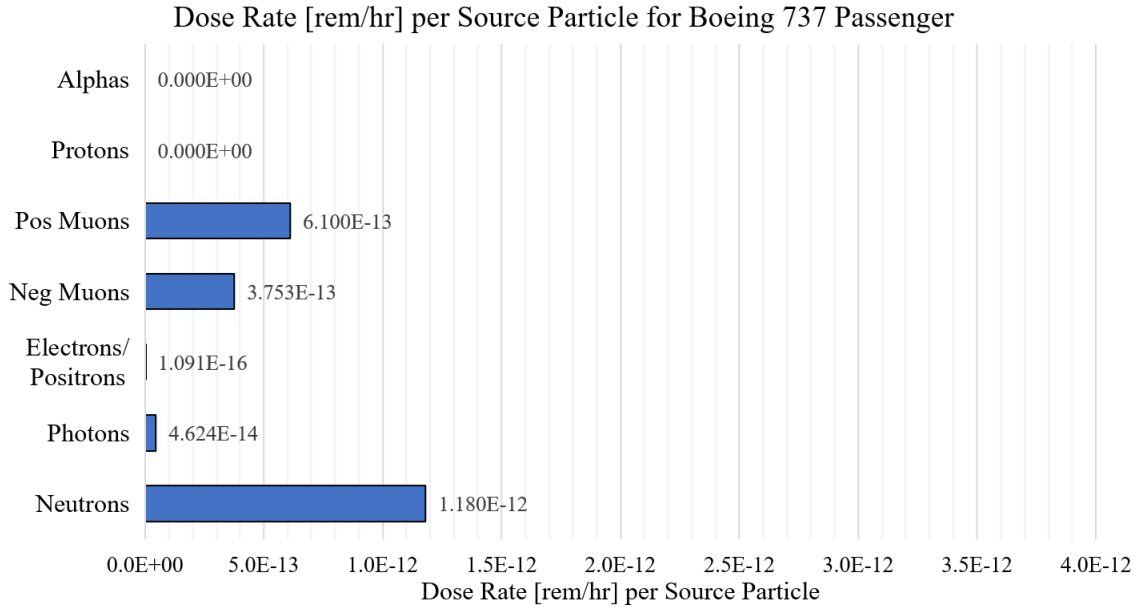

Figure 14: MCNP output of dose rate [rem/hr] per source particle for each type of source (neutrons, photons, electrons/positrons, negative muons, positive muons, protons, and alphas) corresponding to the passenger in row 12 inside the Boeing 737.

4.3 Effective Dose Calculations

To calculate the effective dose received by each aircrew from each flight path, I first converted particle fluence values to number of source particles using Eq. 7, as explained above. Table 4 shows the number of source particle encountered by the A-10 aircraft through each flight path and Table 5 shows the number of source particle encountered by the Boeing 737 aircraft through each flight path. These values only represent the number of source particles met at the outside of each aircraft. Depending on the geometry within the aircraft, the particles that reach the detectors will vary significantly.

Table 4: A-10 Environment - Number of Source Particles from CARI-7A and SIRE2

Date	**Chicago-Reykjavik 01-01-97**	**Chicago-Reykjavik 03-01-01**	**Singapore-Nadi 01-01-97**	**Singapore-Nadi 03-01-01**
Neutrons	$227 \pm 0.1 \times 10^6$	$153 \pm 0.1 \times 10^6$	$87.5 \pm 0.01 \times 10^6$	$79.9 \pm 0.01 \times 10^6$
Photons	$128 \pm 0.1 \times 10^7$	$109 \pm 0.1 \times 10^7$	$153 \pm 0.1 \times 10^7$	$145 \pm 0.1 \times 10^7$
Electrons	$428 \pm 0.1 \times 10^5$	$369 \pm 0.1 \times 10^5$	$544 \pm 0.1 \times 10^5$	$518 \pm 0.1 \times 10^5$
Positrons	$190 \pm 0.1 \times 10^5$	$164 \pm 0.1 \times 10^5$	$242 \pm 0.1 \times 10^5$	$230 \pm 0.1 \times 10^5$
Neg Muons	$342 \pm 0.1 \times 10^4$	$290 \pm 0.1 \times 10^4$	$391 \pm 0.1 \times 10^4$	$367 \pm 0.1 \times 10^4$
Pos Muons	$342 \pm 0.1 \times 10^4$	$290 \pm 0.1 \times 10^4$	$391 \pm 0.1 \times 10^4$	$367 \pm 0.1 \times 10^4$
Protons (GCR)	$109 \pm 0.1 \times 10^5$	$75.3 \pm 0.01 \times 10^5$	$48.1 \pm 0.01 \times 10^5$	$43.9 \pm 0.01 \times 10^5$
Alphas	$1{,}640 \pm 0.01 \times 10^9$	$266{,}000 \pm 0.01 \times 10^9$	0.0	0.0
Protons (SPE)	$17{,}100 \pm 0.01 \times 10^9$	$1{,}350{,}000 \pm 0.001 \times 10^9$	0.0	0.0

Table 5: Boeing 737 Environment - Number of Source Particles from CARI-7A and SIRE2

Date	**Chicago-Reykjavik 01-01-97**	**Chicago-Reykjavik 03-01-01**	**Singapore-Nadi 01-01-97**	**Singapore-Nadi 03-01-01**
Neutrons	$101 \pm 0.05 \times 10^7$	$68.4 \pm 0.05 \times 10^7$	$39 \pm 0.05 \times 10^7$	$35.6 \pm 0.05 \times 10^7$
Photons	$572 \pm 0.5 \times 10^7$	$484 \pm 0.5 \times 10^7$	$681 \pm 0.5 \times 10^7$	$648 \pm 0.5 \times 10^7$
Electrons	$191 \pm 0.05 \times 10^6$	$164 \pm 0.05 \times 10^6$	$242 \pm 0.05 \times 10^6$	$231 \pm 0.05 \times 10^6$
Positrons	$84.8 \pm 0.05 \times 10^6$	$73 \pm 0.05 \times 10^6$	$108 \pm 0.5 \times 10^6$	$103 \pm 0.5 \times 10^6$
Neg Muons	$153 \pm 0.05 \times 10^5$	$129 \pm 0.05 \times 10^5$	$174 \pm 0.05 \times 10^5$	$164 \pm 0.05 \times 10^5$
Pos Muons	$153 \pm 0.05 \times 10^5$	$129 \pm 0.05 \times 10^5$	$174 \pm 0.05 \times 10^5$	$164 \pm 0.05 \times 10^5$
Protons (GCR)	$485 \pm 0.5 \times 10^5$	$336 \pm 0.5 \times 10^5$	$215 \pm 0.5 \times 10^5$	$196 \pm 0.5 \times 10^5$
Alphas	$7{,}290 \pm 0.05 \times 10^9$	$1{,}190{,}000 \pm 0.05 \times 10^9$	0.0	0.0
Protons (SPE)	$76{,}000 \pm 0.05 \times 10^9$	$6{,}020{,}000 \pm 0.05 \times 10^9$	0.0	0.0

Using these values I converted dose rate per source particle to purely dose rate in units of rem per hour. The results are shown in Table 6 for Chicago to Reykjavik on January 1st 1997, Table 7 for Chicago to Reykjavik on March 1st 2001, Table 8 for Singapore to Nadi on January 1st 1997, and Table 9 for Singapore to Nadi on March 1st 2001.

Table 6: Dose Rate [rem/hr] for Aircrew from Chicago to Reykjavik Flight on January 1st 1997

	A-10/Pilot	**Boeing 737/Pilot**	**Boeing 737/Row 12**
Neutrons	$1.68 \pm 0.00915 \times 10^{-4}$	$2.43 \pm 0.0185 \times 10^{-5}$	$1.46 \pm 0.0173 \times 10^{-5}$
Photons	$3.91 \pm 0.0259 \times 10^{-4}$	$4.06 \pm 0.0331 \times 10^{-6}$	$2.78 \pm 0.0284 \times 10^{-6}$
Electrons/ Positrons	$2.97 \pm 0.141 \times 10^{-7}$	$5.53 \pm 0.404 \times 10^{-9}$	$3.03 \pm 0.306 \times 10^{-9}$
Neg Muons	$7.32 \pm 0.113 \times 10^{-6}$	$2.31 \pm 0.0351 \times 10^{-6}$	$1.40 \pm 0.0343 \times 10^{-7}$
Pos Muons	$1.21 \pm 0.0354 \times 10^{-5}$	$3.07 \pm 0.0349 \times 10^{-7}$	$1.80 \pm 0.0348 \times 10^{-7}$
Protons (GCR)	$1.88 \pm 0.235 \times 10^{-7}$	0.0	0.0
Alphas	0.0400 ± 0.005	0.0	0.0
Protons (SPE)	0.295 ± 0.0369	0.0	0.0

Table 7: Dose Rate [rem/hr] for Aircrew from Chicago to Reykjavik Flight on March 1st 2001

	A-10/Pilot	**Boeing 737/Pilot**	**Boeing 737/Row 12**
Neutrons	$1.13 \pm 0.00618 \times 10^{-4}$	$1.64 \pm 0.0125 \times 10^{-5}$	$9.85 \pm 0.117 \times 10^{-6}$
Photons	$3.31 \pm 0.0220 \times 10^{-4}$	$3.43 \pm 0.0280 \times 10^{-6}$	$2.35 \pm 0.0240 \times 10^{-6}$
Electrons/ Positrons	$2.56 \pm 0.122 \times 10^{-7}$	$4.76 \pm 0.348 \times 10^{-9}$	$2.60 \pm 0.262 \times 10^{-9}$
Neg Muons	$6.19 \pm 0.0956 \times 10^{-6}$	$1.95 \pm 0.0296 \times 10^{-7}$	$1.19 \pm 0.0292 \times 10^{-7}$
Pos Muons	$1.02 \pm 0.0125 \times 10^{-5}$	$2.59 \pm 0.0294 \times 10^{-7}$	$1.52 \pm 0.0294 \times 10^{-7}$
Protons (GCR)	$1.30 \pm 0.163 \times 10^{-7}$	0.0	0.0
Alphas	6.50 ± 0.810	0.0	0.0
Protons (SPE)	23.3 ± 2.91	0.0	0.0

Table 8: Dose Rate [rem/hr] for Aircrew from Singapore to Nadi Flight on January 1st 1997

	A-10/Pilot	**Boeing 737/Pilot**	**Boeing 737/Row 12**
Neutrons	$6.45 \pm 0.0358 \times 10^{-5}$	$9.36 \pm 0.0721 \times 10^{-6}$	$5.62 \pm 0.0671 \times 10^{-6}$
Photons	$4.65 \pm 0.0307 \times 10^{-4}$	$4.83 \pm 0.0393 \times 10^{-6}$	$3.31 \pm 0.0337 \times 10^{-6}$
Electrons/ Positrons	$3.77 \pm 0.179 \times 10^{-7}$	$7.03 \pm 0.514 \times 10^{-9}$	$3.84 \pm 0.387 \times 10^{-9}$
Neg Muons	$8.36 \pm 0.129 \times 10^{-6}$	$2.64 \pm 0.0401 \times 10^{-7}$	$1.60 \pm 0.0392 \times 10^{-7}$
Pos Muons	$1.38 \pm 0.0169 \times 10^{-5}$	$3.50 \pm 0.0397 \times 10^{-7}$	$2.05 \pm 0.0397 \times 10^{-7}$
Protons (GCR)	$8.32 \pm 1.04 \times 10^{-8}$	0.0	0.0
Alphas	0.0	0.0	0.0
Protons (SPE)	0.0	0.0	0.0

Table 9: Dose Rate [rem/hr] for Aircrew from Singapore to Nadi Flight on March 1st 2001

	A-10/Pilot	**Boeing 737/Pilot**	**Boeing 737/Row 12**
Neutrons	$5.89 \pm 0.0327 \times 10^{-5}$	$8.54 \pm 0.0660 \times 10^{-6}$	$5.12 \pm 0.0612 \times 10^{-6}$
Photons	$4.42 \pm 0.0292 \times 10^{-4}$	$4.59 \pm 0.0374 \times 10^{-6}$	$3.15 \pm 0.0321 \times 10^{-6}$
Electrons/ Positrons	$3.59 \pm 0.171 \times 10^{-7}$	$6.70 \pm 0.490 \times 10^{-9}$	$3.66 \pm 0.369 \times 10^{-9}$
Neg Muons	$7.84 \pm 0.121 \times 10^{-6}$	$2.47 \pm 0.0375 \times 10^{-7}$	$1.50 \pm 0.0368 \times 10^{-7}$
Pos Muons	$1.29 \pm 0.0158 \times 10^{-5}$	$3.28 \pm 0.0372 \times 10^{-7}$	$1.92 \pm 0.0371 \times 10^{-7}$
Protons (GCR)	$7.59 \pm 0.0949 \times 10^{-8}$	0.0	0.0
Alphas	0.0	0.0	0.0
Protons (SPE)	0.0	0.0	0.0

The flight from Chicago O'Hare International Airport to Keflavik International Airport lasted 5.789 hours while the flight from Singapore Changi Airport to Nadi International Airport was almost twice as long at 10.154 hours. Using these times and Eq. 8 I calculated the effective dose from GCR for each possible passenger intake for all four flight tests.

4.3.1 GCR Effective Dose Results

For each particle of importance I calculated the portion of total effective dose belonging to each one. Figure 15 shows the effective dose received by the A-10 pilot for each GCR particle at the end of all four flights. The photons had a significant influence in the effective dose received by the aircrew on all four flights, even though

after my MCNP runs these particles had one of the lowest dose rate per source particle values. This increase stems from the number of photons meeting the aircraft, i.e. the particle fluence outputs from CARI-7A. Photons had the highest value, at 126 photons per square centimeter, for particle fluence, almost six times higher than the following highest value, neutrons.

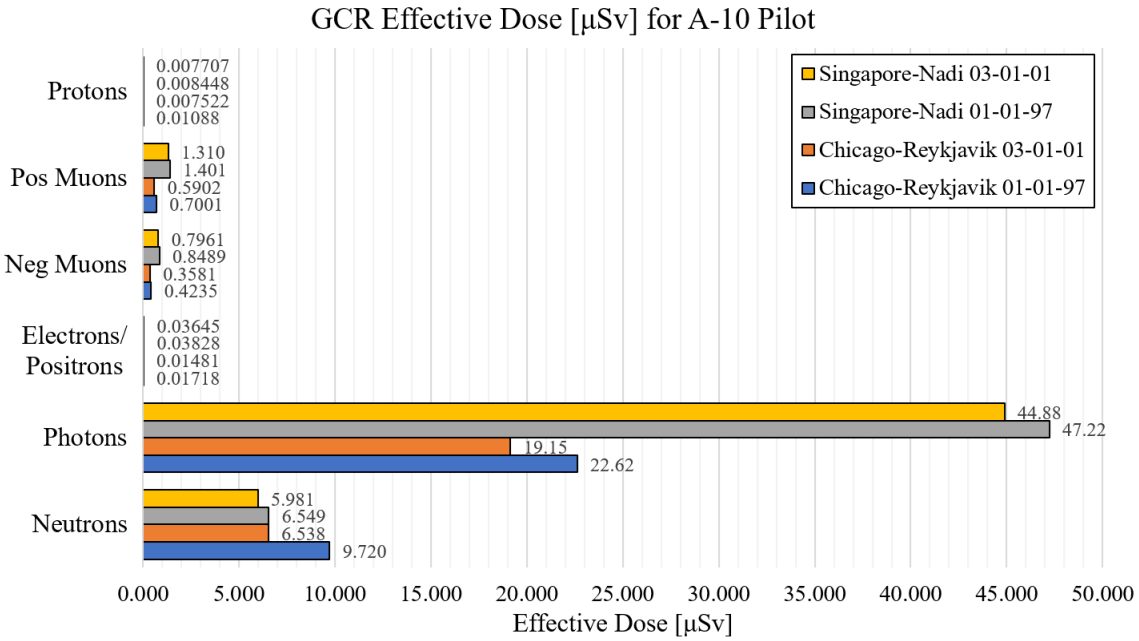

Figure 15: Effective dose for each type of source (neutrons, photons, electrons/-positrons, negative muons, positive muons, and protons) corresponding to the pilot inside the A-10.

Moving on to the Boeing 737 aircraft, both the pilot, shown in Fig. 16, and passenger, shown in Fig. 17, received the majority of their GCR dose from the source photons followed by the neutrons. Although the effective dose from each GCR particle was lower for the passenger in row 12, both the pilot and passenger held similar ratios for the dose contribution of each particle. These dose values do not correspond solely to the particles that made contact with the target detectors, but rather correspond to the original source type from GCR met by the outside of each aircraft. This means that while source neutrons dominated the effective dose values for the pilot

and passenger inside the Boeing 737, the particles that reached the detectors were actually a mix of neutrons, photons and electrons. The original neutrons interact with the matter inside the aircraft and give way to the photons and electrons that eventually make up part of the effective dose calculated by MCNP. For both the A-10 and the Boeing 737 the GCR source particles with the largest influence in effective dose were neutrons and photons.

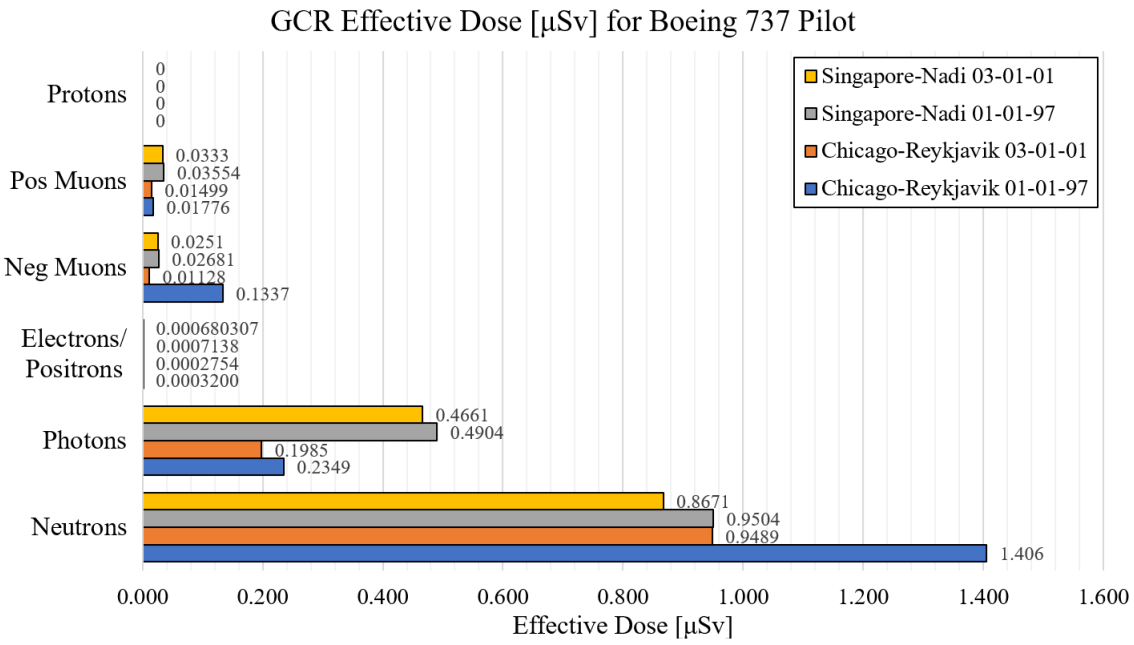

Figure 16: Effective dose for each type of source (neutrons, photons, electrons/-positrons, negative muons, positive muons, and protons) corresponding to the pilot inside the Boeing 737.

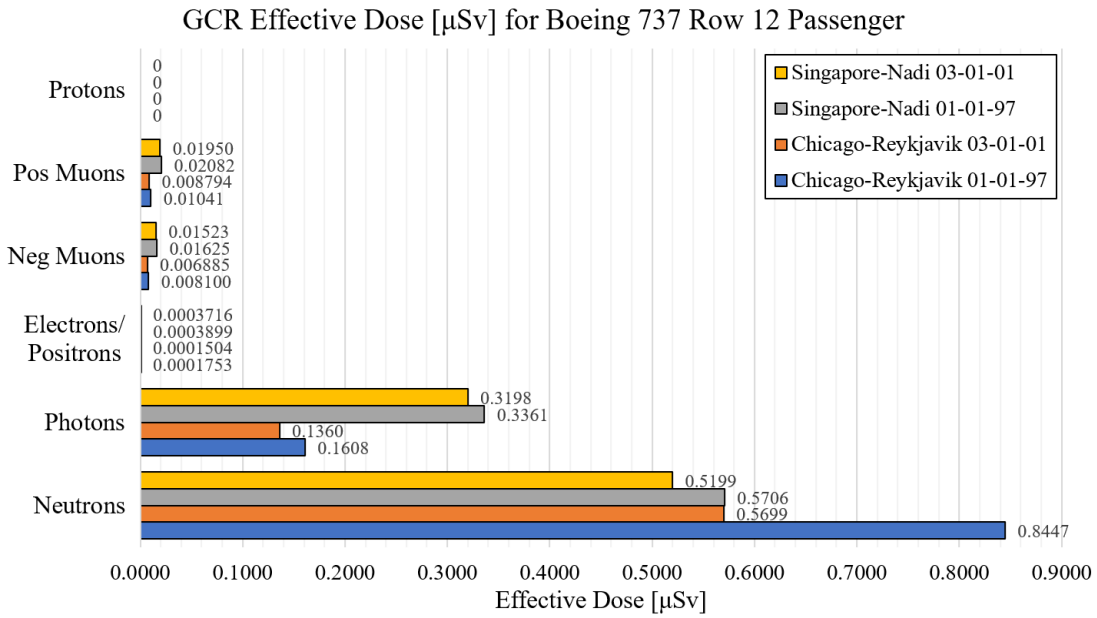

Figure 17: Effective dose for each type of source (neutrons, photons, electrons/-positrons, negative muons, positive muons, and protons) corresponding to the passenger in row 12 inside the Boeing 737.

Table 11 shows the effective dose results from CARI-7A. Compared to the effective dose outputs from this research only certain results matched CARI-7A values. The closest match occurred with a pilot in an A-10 flying from Chicago to Reykjavik. Most calculated effective doses were far off from CARI-7A's results, as shown in the relative error calculations found in Table 12. The geometry for the Boeing 737 plane had substantially more solid material between the source and detectors (pilot and passenger) compared to the A-10 geometry. Additionally, the source particles only carried 1 MeV of energy: this means the once the particles have traveled through this material their ability to reach the detector object is highly limited. In the future adding energy spectra for these sources could increase these numbers to better match the CARI-7A values; however, these results proved that dose intake can change depending on the type of aircraft a person flies or is flying in. Within the A-10 flights, the Singapore to Nadi flight path had effective dose values that varied the most from

CARI-7A results. This flight path is almost twice as long, time wise, than the flight path from Chicago to Reykjavik. In the future testing pairs of flight paths that are around the length to view if there is a pattern between how long the flight is and its relative error relative to CARI-7A results would be useful.

Table 10: GCR Effective Dose [μSv] for Aircrew

	A-10/Pilot	**Boeing 737/Pilot**	**Boeing 737/Row 12**
Chicago-Reykjavik 01-01-97	33.49 ± 0.16	1.793 ± 0.011	1.024 ± 0.010
Chicago-Reykjavik 03-01-01	26.66 ± 0.13	1.174 ± 0.007	0.7217 ± 0.0069
Singapore-Nadi 01-01-97	56.06 ± 0.32	1.504 ± 0.008	0.9442 ± 0.0076
Singapore-Nadi 03-01-01	53.01 ± 0.30	1.392 ± 0.007	0.8748 ± 0.0070

Table 11: GCR Effective Dose [μSv] for Aircrew from CARI-7A

Chicago-Reykjavik 01-01-97	33.6 ± 0.1
Chicago-Reykjavik 03-01-01	24.7 ± 0.1
Singapore-Nadi 01-01-97	22.2 ± 0.1
Singapore-Nadi 03-01-01	20.8 ± 0.1

Table 12: GCR Effective Dose Relative Error Compared to CARI-7A Results

	A-10/Pilot	**Boeing 737/Pilot**	**Boeing 737/Row 12**
Chicago-Reykjavik 01-01-97	100.31%	194.67%	196.95%
Chicago-Reykjavik 03-01-01	107.93%	195.25%	197.08%
Singapore-Nadi 01-01-97	152.53%	193.23%	195.77%
Singapore-Nadi 03-01-01	154.86%	193.31%	195.79%

4.3.1.1 Further Analysis on Particle-Matter Interactions

I conducted analysis on the particle activity within each cell to further understand why the A-10's GCR effective dose was most influenced by photons while the Boeing 737's effective dose was most influenced by neutrons. MCNP's Table 126 [46] gives the user a detailed accounting of the cell's activity including the population within each cell and the average particle track mean free path. I specifically analyzed the cells surrounding the pilot within the A-10 and the pilot within the Boeing 737. I omitted analysis on the passenger within the Boeing 737 since both the pilot and passenger had neutrons as their biggest contributors to effective dose. For the A-10 geometry I selected the cells closest to the pilot including the cockpit front and back, the bottom part of bathtub, and the bottom part of the plane's body (shown in Fig. 18). For the Boeing 737 geometry I selected cells composing the nose and the insulation within the nose (shown in Fig. 19).

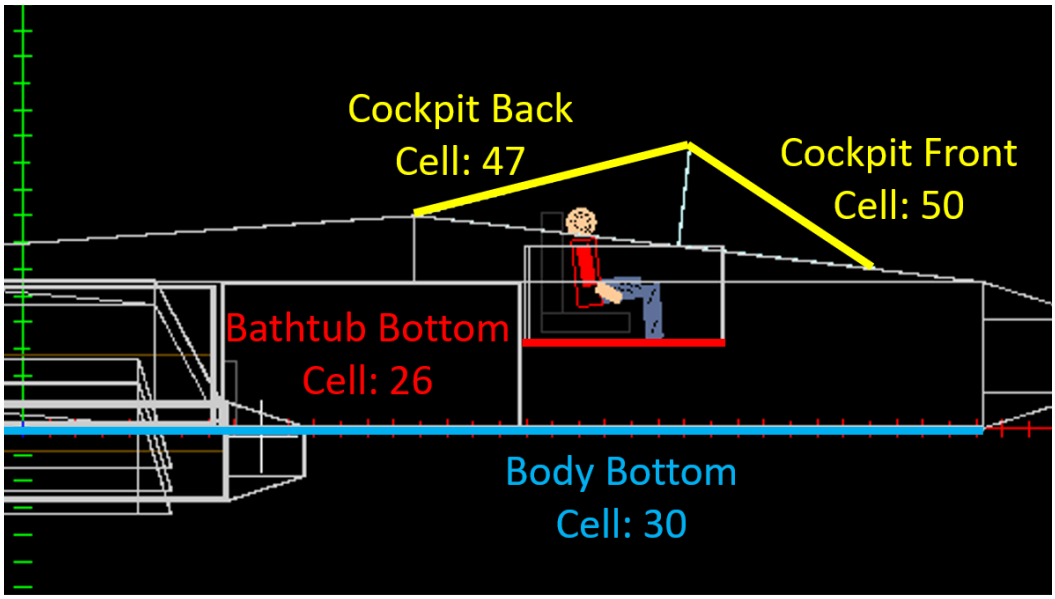

Figure 18: Side view from SWORD's geometry viewer the A-10 aircraft highlighting the cells of importance including the glass cockpit (front and back), the bottom part of titanium bathtub, and the bottom part of the plane's body (made of aluminum).

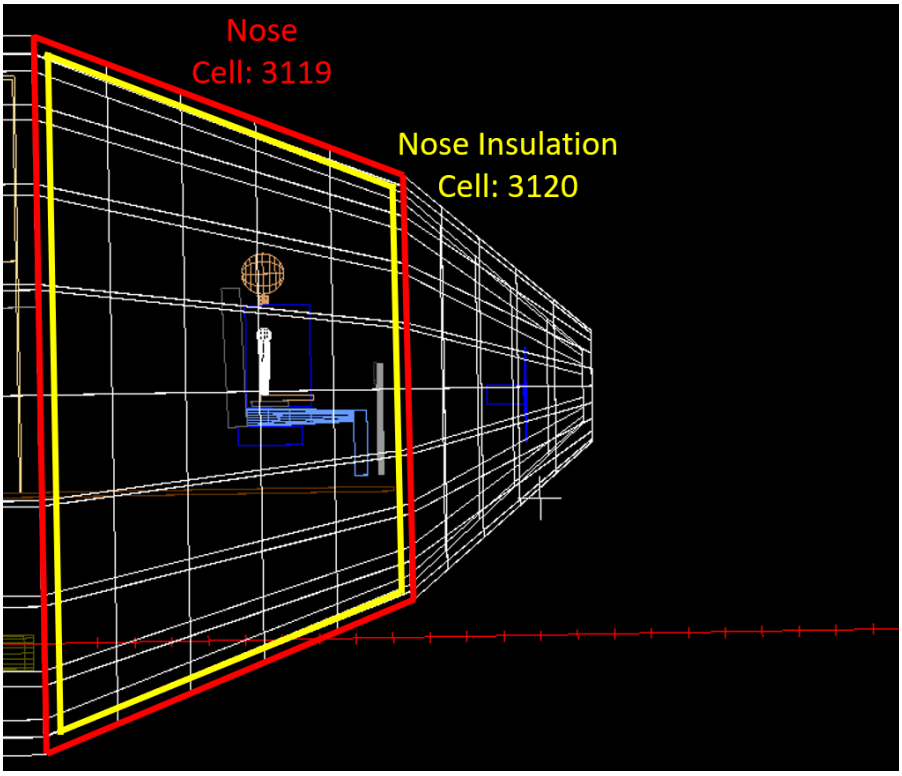

Figure 19: Side view from SWORD's geometry viewer the Boeing 737 aircraft highlighting the cells of importance including the aluminum nose and the nose insulation.

First, I compared the population of particles within the cells for both the neutron and photon source. A high population result represents more particles passing through the material and reaching the pilot. Secondly, I compared the average particle track mean free path for the same two sources. A higher mean free path value result represents higher amounts of shielding and therefore less particles reaching the pilot. As expected, for the A-10 geometry the population values for the photon source were higher than the neutron source (shown in Table 13). Additionally, the mean free path values were higher for the neutron source than the photon source (shown in Table 14) explaining further the photons' significant contribution to the pilot's effective dose value. Comparing these results with the dose rate per source particle for the A-10 pilot (shown in Table 3 and Fig. 12), the neutrons still contributed more to the dose rate than the photons. I believe that the flux to dose conversion factors elevated the neutron contribution; however, when multiplied by the number of source particles (shown in Table 4), photons became the biggest dose contributor. The gap between neutrons and photons in their dose rate per source particle values was not significant compared to the gap between the number of source particles.

Table 13: Population Comparison within A-10 Geometry for Neutron and Photon Sources

	Neutron	**Photon**
Cockpit Front: Cell 50	104,036 ± 2	993,731 ± 1
Cockpit Back: Cell 47	134,495 ± 2	1,216,063 ± 1
Body Bottom: Cell 30	1,250,146 ± 2	2,647,745 ± 1
Bathtub Bottom: Cell 26	395,116 ± 2	2,830,064 ± 1

Table 14: Average Track Mean Free Path [cm] Comparison within A-10 Geometry for Neutron and Photon Sources

	Neutron	**Photon**
Cockpit Front: Cell 50	7.097 ± 0.002	6.450 ± 0.001
Cockpit Back: Cell 47	7.524 ± 0.002	6.296 ± 0.001
Body Bottom: Cell 30	11.900 ± 0.002	5.555 ± 0.001
Bathtub Bottom: Cell 26	7.444 ± 0.002	2.803 ± 0.001

For the Boeing 737 geometry the population values for the photon source were higher than the neutron source (shown in Table 15). Additionally, the mean free path values were higher for the neutron source than the photon source (shown in Table 16). Comparing these results with the dose rate per source particle for the Boeing 737 pilot (shown in Table 3 and Fig. 13), the neutrons contributed more to the dose rate than the photons, with a bigger gap in value than seen with the A-10 pilot. When multiplied by the number of source particles, neutrons remained the biggest dose contributor. It is important to note that even though the pattern between neutron and photon values matched the A-10's results, the effective dose values for the Boeing 737 aircrew were significantly lower than for the A-10 pilot. I recommend further analysis be conducted involving the shielding provided by the materials within the aircraft.

Table 15: Population Comparison within Boeing 737 Geometry for Neutron and Photon Sources

	Neutron	**Photon**
Nose Inner: Cell 3119	706,095 ± 2	3,047,156 ± 1
Nose Insulation: Cell 3120	710,920 ± 2	2,508,691 ± 1

Table 16: Average Track Mean Free Path [cm] Comparison within Boeing 737 Geometry for Neutron and Photon Sources

	Neutron	**Photon**
Nose: Cell 3119	11.163 ± 0.002	5.446 ± 0.001
Nose Insulation: Cell 3120	313.364 ± 0.002	236.484 ± 0.001

4.3.2 SPE Effective Dose Results

The SPE values were more erratic. Because of the lack of SPE particle fluence from the Singapore to Nadi flights as well as the Boeing 737 MCNP dose rates per source particle outputs for protons and alphas, I could only calculate the effective dose received by the A-10 pilot flying from Chicago to Reykjavik, shown in Table 17. The values calculated through my model were far too high, surpassing all annual radiation limits just in one flight. I believe that the fluence values calculated by SIRE2 are high which resulted in these enormous effective dose values. SIRE2 outputs the "free-field" fluence values, which are assumed to represent the same values as CARI-7A since they use the same units and there is no indication in SIRE2's manual of any other meaning for this value. Although the dose values from SIRE2, shown on Table 18, also appear too high, they are not nearly as high as the values I calculated in my model. This comparison in values is shown in Table 19 with each value's relative error relative to SIRE2. Additionally, the dose value from SIRE2 is also expressed as "free field" dose with no indication in its manual of the definition.

Table 17: SPE Effective Dose [μSv] for Aircrew

	A-10/Pilot	**Boeing 737/Pilot**	**Boeing 737/Row 12**
Chicago-Reykjavik 01-01-97	19,400	0.0	0.0
Chicago-Reykjavik 03-01-01	1,730,000	0.0	0.0
Singapore-Nadi 01-01-97	0.0	0.0	0.0
Singapore-Nadi 03-01-01	0.0	0.0	0.0

Table 18: SPE Absorbed Dose [rad] and Effective Dose [μSv] for Aircrew from SIRE2

	Absorbed Dose	**Effective Dose**
Chicago-Reykjavik 01-01-97	2.43 $\pm$ 0.01	2,170 $\pm$ 8.23
Chicago-Reykjavik 03-01-01	259 $\pm$ 1	23,800 $\pm$ 91.9
Singapore-Nadi 01-01-97	0.0	0.0
Singapore-Nadi 03-01-01	0.0	0.0

Table 19: SPE Effective Dose Relative Error Compared to SIRE2 Results

	A-10/Pilot	**Boeing 737/Pilot**	**Boeing 737/Row 12**
Chicago-Reykjavik 01-01-97	793.2%	n/a	n/a
Chicago-Reykjavik 03-01-01	7,144%	n/a	n/a
Singapore-Nadi 01-01-97	n/a	n/a	n/a
Singapore-Nadi 03-01-01	n/a	n/a	n/a

V. Conclusions

5.1 Summary of Findings

In summary, this project integrate all forms of cosmic ionizing radiation in flight-altitude environments into one comprehensive model that outputs dose to military pilots and aircrew within their specific aircraft. Through this research I modeled not only the flight-altitude environments but also particle energy transport through the aircraft until it reached the aircrew. I found that depending on the aircraft's geometry (specifically its size and material components) the dose received by its passengers changes. With the larger, denser Boeing 737 airliner, the effective dose received was less than the dose received by the smaller, lighter A-10 Thunderbolt II. Nevertheless, regardless of material, the GCR source particles with the biggest contribution to effective dose were neutrons and photons for both aircraft. Additionally, I found that position on the aircraft matters. A passenger sitting in the middle of a fully booked aircraft will receive less dose than the pilot in the same aircraft traveling the same flight path. Finally, the results supported correlations between effective dose from GCR, latitude and Sun cycle. Flight paths near the Equator had higher GCR effective dose values than flight paths near the North Pole flying during the same dates. Effective dose values were higher for flights flying during solar minimums than for flights flying during solar maximums on the same flight path. Although some of the results were limiting to the overall analysis of the project, e.g. SPE fluence values for flights near the Equator and proton and alpha dose rates through a Boeing 737, this information marks a significant step forward in assessing and mitigating any potential health risks military aircrew and pilots might endure during flight.

5.2 Future Work

5.2.1 Replacement of SIRE2

Although I was aware that this program was designed for space missions and not commercial flights, I believed that the scope of my project, in terms of location through the atmosphere, still fit inside the scope of SIRE2. The results from this program were either non-existent or far too large in comparison to my other values. While I understand that my methods intended the study of the extreme conditions for SPE, e.g. near the poles during a solar maximum or near the equator during a solar minimum, I still felt these results to be far too extreme to have enough trust in their accuracy to move forward. Additionally, when I conducted my literary review on these different toolkits, I was unable to find any projects that mentioned or even used SIRE2. I believe this was a huge disadvantage since I had no assurance that my outputs from this model were comparable to true results. With CARI-7A there were several papers that not only used the program but also tested its abilities against others of its kind, increasing my confidence on its results. I believe moving forward it would be beneficial to create a software that outputs solely the SPE particle fluence encountered in-flight, specifically designed for commercial and military flight altitudes and paths.

5.2.2 Use of True Energy Spectrum for Particle Sources

One of the biggest downsides of using CARI-7A was the lack of information on the energy spectrum for the particles found at flight altitude. The program was not designed for the purpose of obtaining any information on the individual particles and rather it was meant to output dose values for flights. In several conversations with the creators of CARI-7A, they mentioned future efforts to mend this gap in information with a new program called the Atmospheric Ionizing Radiation Environment Code.

This program is not currently finalized; however, in the upcoming year this code should be available for use by the public. This program is based on the results of the same MCNP calculations that are used in CARI-7A. Although having specific energy spectra for each flight would increase the number of input decks, and therefore the run time needed, it would better represent the environment experienced by the aircrew.

5.2.3 Acquiring True In-Flight Dosimetry Measurements

For this project I compared the effective dose values from my model to the effective dose given by CARI-7A and SIRE2; however, I also used data, particle fluence values, from both programs to calculate those effective dose values. This means that there was no true separation from the comparative values and the outputs of my experiment. Having dosimetry measurements from specific flights that are fully tracked and solely used to test the fidelity of my models would be true measure of the accuracy of the environment I created. The challenge with this proposal is the security implications of having real flight tracks from military aircraft. This would require extensive cooperation between the research team and a specific flight squadron. One option is to work with a pilot training base since their specific flight paths might be easier to acquire in unclassified manner.

5.2.4 Inclusion of TGF Particle Fluences

My project incorporated two out of the three sources of ionizing radiation found at flight altitudes. As explained earlier, for terrestrial gamma flashes, the last source, there was not enough data to effectively model and calculate the dose corresponding to this source. There is a current project in progress regarding equipping WC-130s at the 53rd Weather Reconnaissance Squadron with detectors to measure potential TGFs the planes might come in contact with and where in the atmosphere this occurred.

This data could be added to my currentMCNP input decks to incorporate this source in my environment and fully incorporate all sources of ionizing radiation.

5.2.5 Material Shielding Analysis

Within this research I briefly discussed the materials surrounding the aircraft and its ability to shield the aircrew from radiation; however, military pilots have little say on the aircraft or missions they fly. Therefore, I believe future research should be conducted on shielding materials the pilots and aircrew could wear to reduce their exposure regardless of the type of aircraft. Analysis could be conducted comparing the energy spectra from flight altitude environments and shielding materials to observe if a pilot could fly longer without being exposed to higher amounts of radiation. This could be significant for pregnant pilots or aircrews who continually fly in higher radiation environments.

Appendix

A. A-10 Partial MCNP Input Deck with Neutron Source

```
C Cell Data
C
C  void region
  652   0          1   IMP:N=0 IMP:P=0 IMP:E=0
C A-10 source
  2   6   -1e-25 -2
      3 5 7 16 25
      26 27 28 29 30
      31 32 34 36 37
      38 39 40 41 42
      43 44 45 46 47
      48 49 50 51 52
      53 54 55 62 69
      74 79 82 100 105
      110 115 120 125 130
      131 132 134 159 184
      186 188 189 191 193
      195 197 199 201 202
      204 208 209 210 211
      212 213 214 215 216
      217
      IMP:N=1 IMP:P=1 IMP:E=1
C A-10_BackWing_Left
  3   14   -2.7 -3 4    IMP:N=1 IMP:P=1 IMP:E=1
C A-10_BackWing_Left_Inner
  4   5   -0.00129 -4    IMP:N=1 IMP:P=1 IMP:E=1
C A-10_BackWing_Right
  5   14   -2.7 -5 6    IMP:N=1 IMP:P=1 IMP:E=1
C A-10_BackWing_Right_Inner
  6   5   -0.00129 -6    IMP:N=1 IMP:P=1 IMP:E=1
C A-10_BackWing_Side
  7   5   -0.00129 -7 8 10 12 14    IMP:N=1 IMP:P=1 IMP:E=1
C A-10_BackWing_Side1
  8   14   -2.7 -8 9    IMP:N=1 IMP:P=1 IMP:E=1
C A-10_BackWing_Side1_2
  17   14   -2.7 -17 18    IMP:N=1 IMP:P=1 IMP:E=1

...
C Material Data
C
C WorldVolume material: Vacuum
m6  1001  1
C A-10 material: Air
m5  18040  0.0046615
     6012  0.00016529
     7014  0.78388
     8016  0.21129
```

```
C A-10_BackWing_Left material: Aluminum
m14  13027  1
C A-10_Bathtub_Back material: Titanium
m17  22047  1
C A-10_Cockpit_Back material: Glass
m8  14028  0.33563
     8016  0.66437
C A-10_Engine_Back material: A-10_Engine
m16  13027  0.96446
     26056  0.0023773
     6012  0.033161
C A-10_FuelTank_1 material: Steel
m7  26056  0.95514
     6012  0.044859
C A-10_FuelTank_Aft material: Foam
m13  1001  0.5
     6012  0.5
C A-10_FuelTank_Back_Fuel material: Gasoline_JetFuel
m11  1001  0.69231
     6012  0.30769
C A-10_StockCounterweight material: Lead
m15  82204  0.014
     82206  0.241
     82207  0.221
     82208  0.524
C Cessna-Crew material: Water
m10  1001  0.66667
     8016  0.33333
C
C Output Control Data
C
NPS 50000000
RAND GEN=2 SEED=133113311331133113
C
C Physics Data
C
MODE n p e
MPHYS
PHYS:N 100 0 0 j j j 0 100 j j j 0 0
CUT:N J 1e-7
PHYS:P 100 0 0 -1 0 j 1
PHYS:E 100 0 0 0 0 1 1 1 1 0
C
C Source Data
C
SDEF PAR=N SUR=2 NRM=-1 ERG=1
C
C Tally Data
C
+F16 208 209 210 211 212 213 214 215 216 217 T
DF16 IU=1 FAC=-3 IC=99
C
```

B. Boeing 737 Partial MCNP Input Deck with Photon Source

```
C Cell Data
C
C  void region
  9790   0         1   IMP:P=0 IMP:E=0
C 737 Source
  2   6   -1e-25 -2
      3 3119 3169 3180 3246
      3248 3250 3252 3254 3256
      3258 3260 3262 3 3119
      3169 3180 3246 3248 3250
      3252 3254 3256 3258 3260
      3262 3216 3226 3229 3232
      3234 3236 3239 3242 3244
      3185 3195 3198 3201 3203
      3205 3208 3211 3213 3175
      3177 3179 3114 3116 3118
      3 3119 3169 3180 3246
      3248 3250 3252 3254 3256
      3258 3260 3262 3216 3226
      3229 3232 3234 3236 3239
      3242 3244 3185 3195 3198
      3201 3203 3205 3208 3211
      3213 3175 3177 3179 3114
      3116 3118 3 3119 3169
      3180 3246 3248 3250 3252
      3254 3256 3258 3260 3262
      3216 3226 3229 3232 3234
      3236 3239 3242 3244 3185
      3195 3198 3201 3203 3205
      3208 3211 3213 3175 3177
      3179 3114 3116 3118 3
      3119 3169 3180 3246 3248
      3250 3252 3254 3256 3258
      3260 3262 3216 3226 3229
      3232 3234 3236 3239 3242
      3244 3185 3195 3198 3201
      3203 3205 3208 3211 3213
      3175 3177 3179 3114 3116
      3118
      IMP:P=1 IMP:E=1
C 737-Bag_1_flip_x0_y0_z0
  182   31   -0.15 -182    IMP:P=1 IMP:E=1
C 737-Bag_1_flip_x1_y0_z0
  189   31   -0.15 -189    IMP:P=1 IMP:E=1
C 737-Bag_1_flip_x2_y0_z0
  196   31   -0.15 -196    IMP:P=1 IMP:E=1

...
C Material Data
C
```

```
C WorldVolume material: Vacuum
m6  1001  1
C 737-Bag_1_flip_x0_y0_z0 material: Cotton_clothes-luggage
m31  1001  0.47619
     6012  0.28571
     8016  0.2381
C 737-Central_Fuel material: Aluminum
m21  13027  1
C 737-Central_Fuel_inner material: Air_0
m20  18040  0.0046615
     6012  0.00016529
     7014  0.78388
     8016  0.21129
C 737-Central_Fuel_inner3 material: Gasoline_JetFuel
m14  1001  0.69231
     6012  0.30769
C 737-Chair_armrest material: Foam
m17  1001  0.5
     6012  0.5
C 737-Chair_seat-back material: PE
m16  1001  0.6638
     6012  0.3362
C 737-Engine-Combustor material: Titanium-Allow
m26  13027  0.9424
     22047  0.035412
     23051  0.022183
C 737-Engine-Compressor material: Aluminum_airplane
m27  13027  1
C 737-Fuselage-rib_x0_y0_z0 material: Steel
m7  26056  0.95514
     6012  0.044859
C 737-Fuselage_Insulation material: Fiberglass_insulation
m28  13027  0.04881
     14028  0.18636
     20040  0.092442
     5010  0.010507
     5011  0.0431
     8016  0.61878
C 737-GalleyWall material: Cotton_clothes
m18  1001  0.47619
     6012  0.28571
     8016  0.2381
C 737-Lavatory material: Polyurethane
m12  1001  0.42857
     6012  0.35714
     7014  0.071429
     8016  0.14286
C 737-LeftWheel-rubber material: Rubber-LandingGear
m30  1001  0.61538
     6012  0.38462
C 737-NoseWheel material: Rubber
m15  1001  0.61538
```

```
     6012  0.38462
C 737-Person-Arm_1_c-flip_x0_y0_z0 material: Water
m13  1001  0.66667
     8016  0.33333
C 737-Radar-antenna material: Electronics-PopTop
m25  1001  0.12836
     13027  0.60764
     18040  5.6505e-06
     26056  0.17438
     6012  0.088414
     7014  0.0009502
     8016  0.00025612
C APU material: Engine-APU
m29  13027  0.96446
     26056  0.0023773
     6012  0.033161
C
C Output Control Data
C
NPS 100000000
RAND GEN=2 SEED=133113311331133113
C
C Physics Data
C
MODE p e
MPHYS
PHYS:P 100 0 0 -1 0 j 1
CUT:P J 1e-3
PHYS:E 100 0 0 0 0 1 1 1 1 0
CUT:E J 1e-3
C
C Source Data
C
SDEF PAR=P SUR=2 NRM=-1 ERG=1
C
C Tally Data
C
C Pilot - Row 12 - Flight Attendant
+F16 (3134 3135 3136 3137 3138 3139 3140 3141 3142 3143 3144 3145
   3146)  (683 686 689 692 695 698 701 704 707 710 713 716 719) T
DF16 IU=1 FAC=-3 IC=99
C
```

C. CARI-7A Partial Input for Chicago to Reykjavik Flight on January 01 1997

```
1997/01/01, 0900
DEG MIN N/S DEG MIN E/W FEET TIME(MIN)
41 58.43 N 87 53.53 E 0 0.0
41 58.43 N 87 53.55 E 0 0.25
41 58.42 N 87 53.56 E 0 0.48
41 58.43 N 87 53.58 E 0 0.67
```

```
41 58.43 N 87 53.59 E 0 0.93
41 58.42 N 87 53.6 E 0 2.72
41 58.41 N 87 53.6 E 0 12.4
41 58.4 N 87 53.62 E 0 12.55
41 58.4 N 87 53.63 E 0 12.65
41 58.41 N 87 53.64 E 0 12.72
41 58.42 N 87 53.66 E 0 12.83
41 58.44 N 87 53.66 E 0 12.92
41 58.46 N 87 53.66 E 0 13.03
41 58.48 N 87 53.66 E 0 13.1
41 58.49 N 87 53.68 E 0 13.17
41 58.49 N 87 53.69 E 0 13.22
41 58.48 N 87 53.71 E 0 13.32
41 58.47 N 87 53.72 E 0 13.4
41 58.45 N 87 53.72 E 0 13.47
41 58.44 N 87 53.73 E 0 13.53
41 58.42 N 87 53.74 E 0 13.63
41 58.41 N 87 53.74 E 0 13.7
41 58.4 N 87 53.76 E 0 13.77
41 58.39 N 87 53.78 E 0 13.83
41 58.38 N 87 53.8 E 0 13.9
41 58.38 N 87 53.81 E 0 13.95
41 58.37 N 87 53.82 E 0 14.0
41 58.36 N 87 53.84 E 0 14.05
41 58.36 N 87 53.85 E 0 14.12
41 58.34 N 87 53.9 E 0 14.27
41 58.33 N 87 53.93 E 0 14.35
41 58.33 N 87 53.94 E 0 14.4
41 58.32 N 87 53.96 E 0 14.43
41 58.32 N 87 53.97 E 0 14.47
41 58.32 N 87 54.0 E 0 14.53
41 58.32 N 87 54.01 E 0 14.57
41 58.32 N 87 54.04 E 0 14.63
41 58.32 N 87 54.05 E 0 14.7
41 58.32 N 87 54.07 E 0 14.77
41 58.3 N 87 54.08 E 0 14.85
41 58.28 N 87 54.08 E 0 14.93
41 58.27 N 87 54.08 E 0 15.02
41 58.25 N 87 54.08 E 0 15.08
41 58.24 N 87 54.07 E 0 15.17
41 58.23 N 87 54.05 E 0 15.23
41 58.23 N 87 54.03 E 0 15.33
41 58.23 N 87 54.02 E 0 15.38
41 58.23 N 87 54.0 E 0 15.45
41 58.23 N 87 53.98 E 0 15.5
41 58.23 N 87 53.96 E 0 15.57
41 58.23 N 87 53.95 E 0 15.62
41 58.23 N 87 53.93 E 0 15.65
41 58.23 N 87 53.9 E 0 15.77
41 58.23 N 87 53.88 E 0 15.87
41 58.23 N 87 53.85 E 0 15.95
41 58.23 N 87 53.83 E 0 16.05
```

```
41 58.23 N 87 53.81 E 0 16.15
41 58.23 N 87 53.8 E 0 16.22

...

63 59.03 N 22 36.56 E 0 343.03
63 59.05 N 22 36.57 E 0 343.07
63 59.06 N 22 36.56 E 0 343.12
63 59.07 N 22 36.57 E 0 343.15
63 59.08 N 22 36.57 E 0 343.18
63 59.1 N 22 36.57 E 0 343.22
63 59.12 N 22 36.57 E 0 343.27
63 59.13 N 22 36.57 E 0 343.3
63 59.15 N 22 36.56 E 0 343.35
63 59.19 N 22 36.57 E 0 343.43
63 59.2 N 22 36.57 E 0 343.48
63 59.22 N 22 36.56 E 0 343.52
63 59.26 N 22 36.57 E 0 343.6
63 59.3 N 22 36.57 E 0 343.7
63 59.31 N 22 36.57 E 0 343.73
63 59.35 N 22 36.56 E 0 343.82
63 59.38 N 22 36.57 E 0 343.92
63 59.4 N 22 36.57 E 0 344.02
63 59.43 N 22 36.57 E 0 344.1
63 59.45 N 22 36.57 E 0 344.15
63 59.47 N 22 36.57 E 0 344.27
63 59.49 N 22 36.57 E 0 344.35
63 59.5 N 22 36.58 E 0 344.43
63 59.5 N 22 36.61 E 0 344.5
63 59.5 N 22 36.64 E 0 344.57
63 59.5 N 22 36.66 E 0 344.6
63 59.5 N 22 36.68 E 0 344.63
63 59.5 N 22 36.7 E 0 344.67
63 59.5 N 22 36.72 E 0 344.7
63 59.5 N 22 36.74 E 0 344.73
63 59.5 N 22 36.76 E 0 344.75
63 59.5 N 22 36.77 E 0 344.78
63 59.5 N 22 36.79 E 0 344.8
63 59.5 N 22 36.81 E 0 344.82
63 59.5 N 22 36.82 E 0 344.83
63 59.5 N 22 36.96 E 0 345.0
63 59.5 N 22 37.05 E 0 345.1
63 59.5 N 22 37.14 E 0 345.2
63 59.5 N 22 37.21 E 0 345.28
63 59.5 N 22 37.3 E 0 345.38
63 59.5 N 22 37.39 E 0 345.5
63 59.5 N 22 37.47 E 0 345.58
63 59.5 N 22 37.53 E 0 345.7
63 59.5 N 22 37.57 E 0 345.78
63 59.51 N 22 37.58 E 0 345.82
63 59.51 N 22 37.6 E 0 345.87
63 59.53 N 22 37.61 E 0 345.95
63 59.54 N 22 37.61 E 0 346.02
```

```
63 59.55 N 22 37.63 E 0 346.07
63 59.57 N 22 37.64 E 0 346.13
63 59.59 N 22 37.65 E 0 346.25
63 59.6 N 22 37.65 E 0 346.32
63 59.63 N 22 37.64 E 0 346.45
63 59.64 N 22 37.63 E 0 346.52
63 59.64 N 22 37.61 E 0 346.57
63 59.64 N 22 37.6 E 0 346.62
63 59.63 N 22 37.58 E 0 346.68
63 59.63 N 22 37.57 E 0 346.75
63 59.63 N 22 37.55 E 0 346.82
63 59.63 N 22 37.54 E 0 346.9
63 59.62 N 22 37.53 E 0 347.15
```

D. SIRE2 Partial Input for Singapore to Nadi Flight on March 01 2001

```
SIRE2 input file


       Time (UTCG)           Lat (deg)    Lon (deg)     Alt (km)
   Lat Rate (deg/sec)    Lon Rate (deg/sec)    Alt Rate (km/sec)
-------------------------    ---------    ---------    ----------
   ------------------    ------------------    -----------------
01 Mar 2001 09:00:00.000    1.365      103.995      0.000000
    0.0001               0.0001                0.0001
01 Mar 2001 09:00:06.000    1.365      103.995      0.000000
    0.0001               0.0001                0.0001
01 Mar 2001 09:01:25.000    1.365      103.998      0.000000
    0.0001               0.0001                0.0001
01 Mar 2001 09:01:33.000    1.365      103.998      0.000000
    0.0001               0.0001                0.0001
01 Mar 2001 09:01:39.000    1.365      103.999      0.000000
    0.0001               0.0001                0.0001
01 Mar 2001 09:01:45.000    1.366      103.999      0.000000
    0.0001               0.0001                0.0001
01 Mar 2001 09:01:50.000    1.366      103.999      0.000000
    0.0001               0.0001                0.0001
01 Mar 2001 09:01:55.000    1.366      103.999      0.000000
    0.0001               0.0001                0.0001
01 Mar 2001 09:02:01.000    1.367      103.999      0.000000
    0.0001               0.0001                0.0001
01 Mar 2001 09:02:05.000    1.367      103.999      0.000000
    0.0001               0.0001                0.0001
01 Mar 2001 09:02:09.000    1.367      103.999      0.000000
    0.0001               0.0001                0.0001
01 Mar 2001 09:02:13.000    1.367      103.999      0.000000
    0.0001               0.0001                0.0001
01 Mar 2001 09:02:19.000    1.368      104.000      0.000000
    0.0001               0.0001                0.0001
01 Mar 2001 09:02:25.000    1.368      104.000      0.000000
    0.0001               0.0001                0.0001
```

```
...
01 Mar 2001 19:06:21.000    -17.752      177.446      0.000000
      0.0001               0.0001                    0.0001
01 Mar 2001 19:06:27.000    -17.752      177.446      0.000000
      0.0001               0.0001                    0.0001
01 Mar 2001 19:06:33.000    -17.751      177.446      0.000000
      0.0001               0.0001                    0.0001
01 Mar 2001 19:06:38.000    -17.751      177.447      0.000000
      0.0001               0.0001                    0.0001
01 Mar 2001 19:06:43.000    -17.751      177.447      0.000000
      0.0001               0.0001                    0.0001
01 Mar 2001 19:06:49.000    -17.751      177.447      0.000000
      0.0001               0.0001                    0.0001
01 Mar 2001 19:06:54.000    -17.751      177.447      0.000000
      0.0001               0.0001                    0.0001
01 Mar 2001 19:06:58.000    -17.751      177.448      0.000000
      0.0001               0.0001                    0.0001
01 Mar 2001 19:07:03.000    -17.751      177.448      0.000000
      0.0001               0.0001                    0.0001
01 Mar 2001 19:07:10.000    -17.751      177.448      0.000000
      0.0001               0.0001                    0.0001
01 Mar 2001 19:07:16.000    -17.752      177.449      0.000000
      0.0001               0.0001                    0.0001
01 Mar 2001 19:07:22.000    -17.752      177.449      0.000000
      0.0001               0.0001                    0.0001
01 Mar 2001 19:07:34.000    -17.752      177.449      0.000000
      0.0001               0.0001                    0.0001
01 Mar 2001 19:07:44.000    -17.752      177.449      0.000000
      0.0001               0.0001                    0.0001
01 Mar 2001 19:07:53.000    -17.752      177.449      0.000000
      0.0001               0.0001                    0.0001
01 Mar 2001 19:08:03.000    -17.752      177.449      0.000000
      0.0001               0.0001                    0.0001
01 Mar 2001 19:08:12.000    -17.752      177.449      0.000000
      0.0001               0.0001                    0.0001
01 Mar 2001 19:08:21.000    -17.753      177.450      0.000000
      0.0001               0.0001                    0.0001
01 Mar 2001 19:08:32.000    -17.753      177.450      0.000000
      0.0001               0.0001                    0.0001
01 Mar 2001 19:08:43.000    -17.753      177.450      0.000000
      0.0001               0.0001                    0.0001
01 Mar 2001 19:09:14.000    -17.753      177.450      0.000000
      0.0001               0.0001                    0.0001
```

Bibliography

1. Federal Aviation Administration. Advisory circular no. 120-61, may 19, 1994. crewmember training on in-flight radiation exposure, 1994.

2. Wallace Friedberg, Kyle Copeland, et al. What aircrews should know about their occupational exposure to ionizing radiation. Technical report, United States. Department of Transportation. Federal Aviation Administration ..., 2003.

3. Occupational Safety and Health Administration. Ionizing radiation. `https://www.osha.gov/ionizing-radiation/health-effects`, accessed on: 08-01-22.

4. Jean-Francois Bottollier-Depois, Peter Beck, Marcin Latocha, Vladimir Mares, D Matthiä, W Rühm, and Frank Wissmann. Comparison of codes assessing radiation exposure of aircraft crew due to galactic cosmic radiation. *EURADOS report*, 3:2012, 2012.

5. National Oceanic and Atmospheric Administration. Galactic cosmic rays. `https://www.swpc.noaa.gov/phenomena/galactic-cosmic-rays`, accessed on: 07-01-22.

6. DT Bartlett. Radiation protection aspects of the cosmic radiation exposure of aircraft crew. *Radiation protection dosimetry*, 109(4):349–355, 2004.

7. Natalya A. Kilifarska, Volodymyr G. Bakhmutov, and Galyna V. Melnyk. Chapter 5 - galactic cosmic rays and solar particles in earth's atmosphere. In Natalya A. Kilifarska, Volodymyr G. Bakhmutov, and Galyna V. Melnyk, editors, *The Hidden Link between Earth's Magnetic Field and Climate*, pages 101–131. Elsevier, 2020.

8. Honglu Wu, Janice L Huff, Rachel Casey, Myung-Hee Kim, and Francis A Cucinotta. Risk of acute radiation syndromes due to solar particle events. *The Human Health and Performance Risks for Space Explorations. Houston, Texas: NASA Human Research Program*, pages 171–90, 2009.

9. Shaowen Hu. Solar particle events and radiation exposure in space. *NASA Space Radiation Program Element, Human Research Program*, pages 1–15, 2017.

10. MA Shea, DF Smart, KG McCracken, GAM Dreschhoff, and Harlan E Spence. Solar proton events for 450 years: The carrington event in perspective. *Advances in Space Research*, 38(2):232–238, 2006.

11. Freddy Moreno Cárdenas, Sergio Cristancho Sánchez, and Santiago Vargas Domínguez. The grand aurorae borealis seen in colombia in 1859. *Advances in Space Research*, 57(1):257–267, 2016.

12. Joseph R Dwyer, David M Smith, and Steven A Cummer. High-energy atmospheric physics: Terrestrial gamma-ray flashes and related phenomena. *Space Science Reviews*, 173(1):133–196, 2012.

13. Joseph R Dwyer and Martin A Uman. The physics of lightning. *Physics Reports*, 534(4):147–241, 2014. The Physics of Lightning.

14. Gaopeng Lu, Richard J Blakeslee, Jingbo Li, David M Smith, Xuan-Min Shao, Eugene W McCaul, Dennis E Buechler, Hugh J Christian, John M Hall, and Steven A Cummer. Lightning mapping observation of a terrestrial gamma-ray flash. *Geophysical Research Letters*, 37(11), 2010.

15. US Inan, MB Cohen, RK Said, DM Smith, and LI Lopez. Terrestrial gamma ray flashes and lightning discharges. *Geophysical research letters*, 33(18), 2006.

16. Jeri L Anderson, Christopher J Mertens, Barbara Grajewski, Lian Luo, Chih-Yu Tseng, and Rick T Cassinelli. Flight attendant radiation dose from solar particle events. *Aviation, Space, and Environmental Medicine*, 85(8):828–832, 2014.

17. József Kóta. Theory and modeling of galactic cosmic rays: Trends and prospects. *Space Science Reviews*, 176(1):391–403, 2013.

18. Matthias M Meier, Kyle Copeland, Daniel Matthiä, Christopher J Mertens, and Kai Schennetten. First steps toward the verification of models for the assessment of the radiation exposure at aviation altitudes during quiet space weather conditions. *Space Weather*, 16(9):1269–1276, 2018.

19. Peter Beck, DT Bartlett, Pawel Bilski, Clive Dyer, Erwin Flückiger, Nicolas Fuller, Pierre Lantos, Günther Reitz, Werner Rühm, Frantisek Spurny, et al. Validation of modelling the radiation exposure due to solar particle events at aircraft altitudes. *Radiation protection dosimetry*, 131(1):51–58, 2008.

20. Kyle Copeland. CARI-7A: Development and validation. *Radiation Protection Dosimetry*, 175(4):419–431, 2017.

21. JH Adams Jr, ZD Robinson, JH Nonnast, JH Fisher, DM Hope, ZB Lane, RA Reed, JZ Fisher, KM Warren, and BD Sierawski. The SIRE2 toolkit. *Space Weather*, 18(7):e2019SW002364, 2020.

22. William Nichols. Flying duties while pregnant policy clarification. `https://mypers.af.mil/app/answers/detail/a_id/52402`, accessed on: 02-27-22, Apr 2022.

23. Exposure (radiation). `https://www.nrc.gov/reading-rm/basic-ref/glossary/exposure.html`, accessed on: 03-08-23, Feb 2023.

24. Radiological Society of North America (RSNA) and American College of Radiology (ACR). What is radiation dose? https://www.radiologyinfo.org/en/info/safety-hiw_09, accessed on 03-08-23, Apr 2022.

25. Dose (radiation). https://www.nrc.gov/reading-rm/basic-ref/glossary/dose.html, accessed on: 03-08-23, Feb 2023.

26. Thomas K Gaisser, Ralph Engel, and Elisa Resconi. *Cosmic rays and particle physics*. Cambridge University Press, 2016.

27. Elena Amato. The origin of galactic cosmic rays. *International Journal of Modern Physics D*, 23(07):1430013, 2014.

28. The European Organization for Nuclear Research (CERN). Cosmic rays: Particles from outer space. https://home.cern/science/physics/cosmic-rays-particles-outer-space, accessed on: 11-01-22.

29. ICRP. *ICRP publication 60: 1990 recommendations of the International Commission on Radiological Protection*. Number 60. Elsevier Health Sciences, 1991.

30. Kyle Copeland et al. CARI-7A documentation: User's guide. Technical report, United States Department of Transportation Federal Aviation Administration, 2021.

31. P M O'Neill and M Y Kim. Badhwar-O'Neill 2011 galactic cosmic ray model update and future improvements. In *NASA Space Radiation Investigators Workshop*, number JSC-CN-29864, 2014.

32. P M O'Neill, S Golge, and T C Slaba. Badhwar-O'Neill 2014 galactic cosmic ray flux model description. Technical report, 2015.

33. Kyle Copeland et al. CARI-7 documentation: Particle spectra. Technical report, United States Department of Transportation Federal Aviation Administration, 2021.

34. P Lantos. Forbush decrease effects on radiation dose received on-board aeroplanes. *Radiation protection dosimetry*, 117(4):357–364, 2005.

35. Tony C Slaba and Kathryn Whitman. The Badhwar-O'Neill 2020 GCR model. *Space Weather*, 18(6):e2020SW002456, 2020.

36. ICRP. *ICRP publication 103: 2003 recommendations of the International Commission on Radiological Protection*. Number 103. Elsevier Health Sciences, 2007.

37. Kyle A Copeland et al. *Cosmic ray particle fluences in the atmosphere resulting from primary cosmic ray heavy ions and their resulting effects on dose rates to aircraft occupants as calculated with MCNPX 2.7.0*. PhD thesis, 2014.

38. Darrell R Fisher and Frederic H Fahey. Appropriate use of effective dose in radiation protection and risk assessment. *Health physics*, 113(2):102, 2017.

39. CB Meinhold, S Abraharnson, SJ Adelstein, et al. Report no. 116—limitation of exposure to ionizing radiation (supersedes ncrp report no. 91). *Bethesda, MD: National Council on Radiation Protection & Measurements*, 1993.

40. William R Webber, JR Benbrook, JR Thomas, Al Hunting, and Richard Duncan. An evaluation of the radiation hazard due to solar-particle events. Technical report, BOEING AEROSPACE CO SEATTLE WA, 1963.

41. Christopher J Mertens, Brian T Kress, Michael Wiltberger, Steve R Blattnig, Tony S Slaba, Stanley C Solomon, and M Engel. Geomagnetic influence on aircraft radiation exposure during a solar energetic particle event in october 2003. *Space Weather*, 8(3), 2010.

42. Jonathan H Fisher, Jim Adams, Joseph Nonnast, Zachary Robinson, Jonathan Z Fisher, Jeren Suzuki, Paul Boberg, Wally Westlake, and Haley Cole. *Space Ionizing Radiation Environments and Effects (SIRE2) User Guide*. Fifth Gait Technologies.

43. Flightradar24. Live flight tracker - real-time flight tracker map. `https://www.flightradar24.com/how-it-works`, accessed on: 10-01-22.

44. The MCNP code. `https://mcnp.lanl.gov/`, accessed on 03-09-23, Jan 2023.

45. *SWORD Reference Guide*.

46. CJ Werner, J Armstrong, FB Brown, JS Bull, L Casswell, LJ Cox, D Dixon, RA Forster, JT Goorley, HG HUghes, J Favorite, R Martz, SG Mashnik, Rising ME, CJ Solomon, A Sood, JE Sweezy, A Zukaitis, C Anderson, JS Elson, JW Durkee, RC Johns, GW McKinney, GE McMath, JS Hendricks, DB Pelowitz, RE Prael, TE Booth, MR James, ML Fensin, TA Wilcox, and BC Kiedrowski. *MCNP User's Manual Code Version 6.2 Guide*. Los Alamos National Labpratories.

47. Ronald J McConn, Christopher J Gesh, Richard T Pagh, Robert A Rucker, and Robert Williams III. Compendium of material composition data for radiation transport modeling. Technical report, Pacific Northwest National Lab (PNNL), Richland, WA (United States), 2011.

48. Michael F L'Annunziata. Nuclear radiation, its interaction with matter and radioisotope decay. *Handbook of Radioactivity Analysis*, pages 1–122, 2003.

Acronyms

BO11 Badhwar and O'Neill 2011. 12

BO14 Badhwar and O'Neill 2014. 12

BO20 Badhwar and O'Neill 2020. 12

CARI Civil Aviation Research Institute. 12, 15

CARI-7A Civil Aviation Research Institute -7A software. viii, 5, 6, 12, 13, 14, 16, 17, 19, 21, 25, 26, 31, 34, 40, 41, 42, 43, 54, 56, 57, 62, 66, 67

CCMC Community Coordinated Modeling Center. 16

CMES Coronal Mass Ejection Shocks. 3

CREME Cosmic Ray Effects on Microelectronics. 20, 27

DLR German Aerospace Center. 16

Dst Disturbance Storm Time Index. 20

FAA Federal Aviation Administration. 1, 12, 16

GCR Galactic Cosmic Radiation. 2, 5, 9, 10, 12, 13, 14, 16, 17, 18, 19, 25, 31, 38, 41, 42, 53, 54, 55, 58, 65

GUI Guided User Interface. 21, 25, 27

ICRP International Commission on Radiological Protection. 13, 15, 26, 35, 36

ISO International Standards Organization. 12

Kp Planetary K-index. 20, 27

MCNP Monte Carlo N-Particle Transport Code. vi, ix, 6, 12, 26, 27, 28, 30, 31, 32, 33, 34, 35, 36, 38, 43, 44, 54, 55, 58, 62, 67, 68

NAIRAS Nowcast of Atmospheric Ionizing Radiation for Aviation Safety. 19

NASA National Aeronautics and Space Administration. 12, 16

NCRP National Council on Radiation Protection. 15

NIOSH National Institute for Occupational Safety and Health. 18

NOAA National Oceanic and Atmospheric Administration. 19

SF Solar Flare. 3

SIRE2 Space Ionizing Radiation Environment and Effects toolkit. vi, viii, 5, 6, 20, 21, 22, 25, 26, 27, 34, 40, 41, 42, 43, 62, 66, 67

SPE Solar Particle Events. vi, 2, 3, 5, 17, 18, 19, 20, 26, 27, 39, 41, 43, 62, 65, 66

SWORD Software for Optimization of Radiation Detectors. vi, viii, 6, 27, 28, 29, 30, 31

TGF Terrestrial Gamma Flash. 3, 4, 6, 7, 67

REPORT DOCUMENTATION PAGE

Form Approved
OMB No. 0704–0188

1. REPORT DATE *(DD–MM–YYYY)*	2. REPORT TYPE	3. DATES COVERED *(From — To)*
23–03–2023	Master's Thesis	Sept 2021 — Mar 2023

4. TITLE AND SUBTITLE

Modeling Radiation Exposure on Flight Missions to Analyze Aircrew Risk

5a. CONTRACT NUMBER

5b. GRANT NUMBER

5c. PROGRAM ELEMENT NUMBER

6. AUTHOR(S)

Quintero Hilsaca, Camila V., 2nd Lt, USAF

5d. PROJECT NUMBER

5e. TASK NUMBER

5f. WORK UNIT NUMBER

7. PERFORMING ORGANIZATION NAME(S) AND ADDRESS(ES)

Air Force Institute of Technology
Graduate School of Engineering and Management (AFIT/EN)
2950 Hobson Way
WPAFB OH 45433-7765

8. PERFORMING ORGANIZATION REPORT NUMBER

AFIT-ENP-MS-23-M-101

9. SPONSORING / MONITORING AGENCY NAME(S) AND ADDRESS(ES)

Air Force Research Laboratory
711 HPW USAFSAM/OEC
Wright-Patterson AFB OH 45433-7765
ATTN: William J. Erwin
Email: william.erwin.2@us.af.mil

10. SPONSOR/MONITOR'S ACRONYM(S)

USAFSAM

11. SPONSOR/MONITOR'S REPORT NUMBER(S)

12. DISTRIBUTION / AVAILABILITY STATEMENT

DISTRIBUTION STATEMENT A:
APPROVED FOR PUBLIC RELEASE; DISTRIBUTION UNLIMITED.

13. SUPPLEMENTARY NOTES

14. ABSTRACT

GCR and SPE comprise the majority of the ionizing radiation experienced in the upper atmosphere within flight-altitude environments. Although previous studies have analyzed radiation doses from single sources on civilian flight operations, there is a lack of research focused on dose received by military personnel during flight from both sources simultaneously. In-flight radiation environments are modeled through the MCNP6 for two separate aircraft, an Air Force A-10 and a Boeing 737. Particle fluence values for galactic cosmic rays and solar particle events for four separate flight paths are determined using the CARI-7A software and the SIRE2 toolkit, respectively. MCNP6 code and flux-to-dose conversion factors from the ICRP Pub. 60 were used to determine the effective dose received by aircrew. The effective dose for each flight was compared to the effective dose provided by CARI-7A and SIRE2. Overall, the results for GCR and SPE doses through the simulated environment matched CARI-7A results better than SIRE2 results. SIRE2 predicted no particle fluence for the two flight tracks through the equator and an effective dose of 23,760 μSv for a flight path near the Arctic circle during a solar maximum. Additionally, for the Boeing 737 the effective dose for a passenger in the middle of the plane was approximately half of the effective dose for the pilot at the front of the aircraft. Finally, a A-10 pilot received approximately 10 times the dose of a Boeing 737 pilot.

15. SUBJECT TERMS

CARI-7A, galactic cosmic radiation (GCR), effective dose, flight missions, ionizing radiation, MCNP6, military aircrew, particle transport, radiation risk, SIRE2, solar particle events (SPE), SWORD

16. SECURITY CLASSIFICATION OF:			17. LIMITATION OF ABSTRACT	18. NUMBER OF PAGES	19a. NAME OF RESPONSIBLE PERSON
a. REPORT	b. ABSTRACT	c. THIS PAGE			Dr. John McClory, AFIT/ENP
U	U	U	UU	99	19b. TELEPHONE NUMBER *(include area code)* (937) 255-6565; john.mcclory@afit.edu